INVESTIGATION OF THE FEASIBILITY OF THE ELECTRON BEAM-EXCITED, HIGH PRESSURE RECOMBINATION LASER

Carl B. Collins, et al

Texas University at Dallas

Prepared for:

Office of Naval Research
Advanced Research Projects Agency

1 August 1974

Security Classification

DOCUMENT CONTROL DATA - R & D

AD 786 738

(Security classification of title, body of abstract and indexing annotation must be entered when the overall report is classified)

1 ORIGINATING ACTIVITY (Corporate author)

The University of Texas at Dallas
P. O. Box 688
Richardson, Texas 75080

2a. REPORT SECURITY CLASSIFICATION

UNCLASSIFIED

2b. GROUP

3 REPORT TITLE

INVESTIGATION OF THE FEASIBILITY OF THE ELECTRON BEAM-EXCITED, HIGH PRESSURE RECOMBINATION LASER

4 DESCRIPTIVE NOTES (Type of report and inclusive dates)

Special Technical Report

5 AUTHOR(S) (First name, middle initial, last name)

Carl B. Collins

Austin J. Cunningham

6 REPORT DATE

1, August 1974

7a. TOTAL NO OF PAGES

79

7b. NO OF REFS

21

8a. CONTRACT OR GRANT NO

N00014-67-A-0310-0007

b. PROJECT NO

ARPA Order No. 1807

c. Program Code 2E90

d

9a. ORIGINATOR'S REPORT NUMBER(S)

UTDP - ML - 01

9b. OTHER REPORT NO(S) (Any other numbers that may be assigned this report)

10 DISTRIBUTION STATEMENT

Distribution of this document is unlimited

11 SUPPLEMENTARY NOTES

12 SPONSORING MILITARY ACTIVITY

Office of Naval Research

13 ABSTRACT

The first nitrogen ion laser pumped by charge transfer from He_2^+ is reported in this work. Intense laser emission in the violet at 427 nm has been observed and found to have a linewidth less than 0.3 nm. The pumping ion, He_2^+, was produced by discharge of a fast-pulsed electron beam gun, APEX-1, into 7 atmospheres of a mixture of helium and nitrogen. Excitation current densities were 1.4 KA/cm^2 at 1 MV over a 1 x 10 cm transverse geometry. Under these conditions, the efficiency of the emission of 427 nm laser radiation was found to be 1.8% relative to the energy lost by the electron beam in the radiating volume.

DD FORM 1 NOV 1473

Security Classification

14 KEY WORDS	LINK A		LINK B		LINK C	
	ROLE	WT	ROLE	WT	ROLE	WT
Nitrogen Ion Laser						
Charge Transfer						
Laser						

Special Technical Report

on

THE NITROGEN ION LASER

Short Title: RECOMBINATION LASER

ARPA Order Number 1807

Program Code Number 2E90

Contract Number N00014-67-A0310-0007

Principal Investigator: C. B. Collins
The University of Texas at Dallas
P. O. Box 688
Richardson, Texas 75080
(214) 690-2885

Contractor: The Board of Regents of
The University of Texas System

Scientific Officer: Director
Physics Programs
Physical Sciences Division
Office of Naval Research
Department of the Navy
800 N. Quincy Street
Arlington, Virginia 22217

Effective Date of Contract : 21 March 1972

Expiration Date of Contract : 30 July 1975

Amount of Contract	:	$ 99,990.00
Amount of Modification #1	:	91,400.00
Amount of Modification #2	:	100,000.00
Amount of Modification #3	:	150,000.00
Total Amount	:	$441,390.00

Sponsored by

Advanced Research Projects Agency

ARPA Order No. 1807

Form Approved Budget Bureau No. 22-R0293

CONTENTS

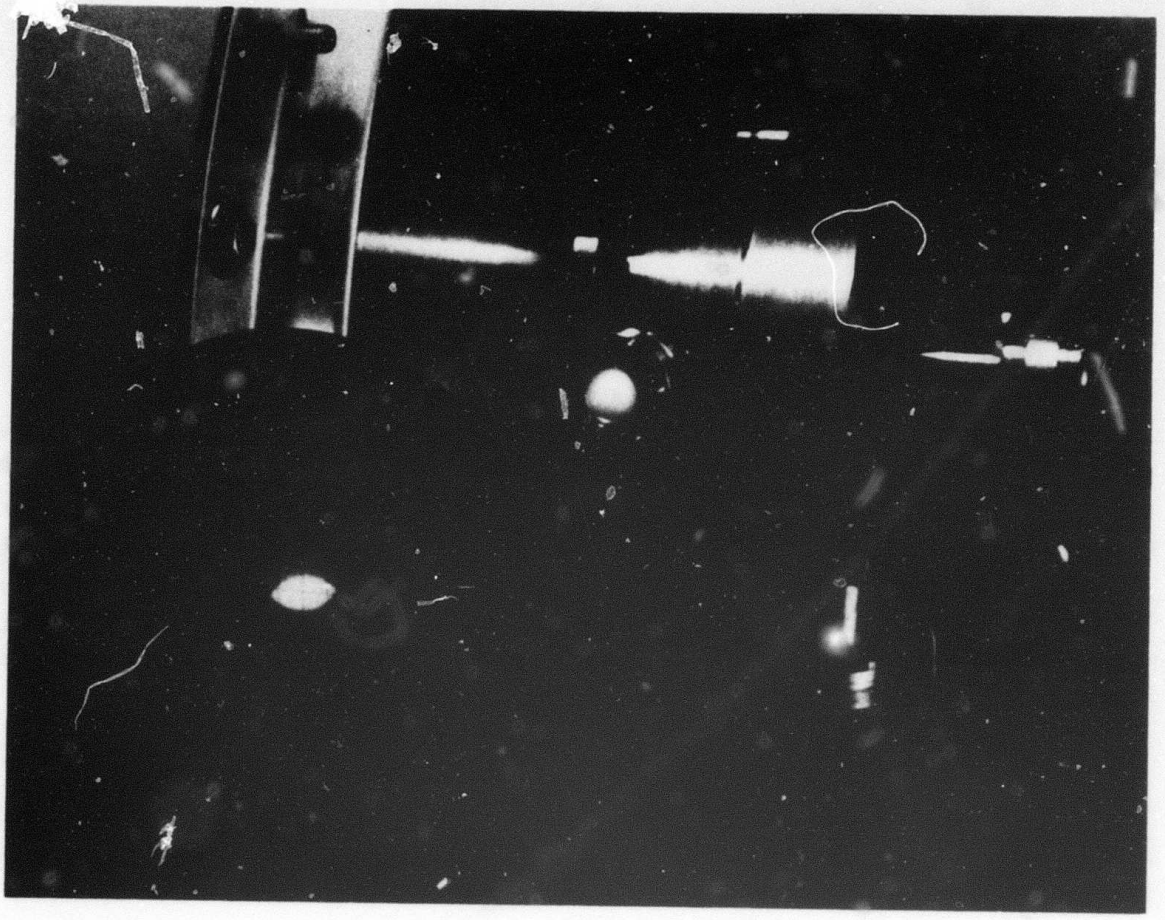

Emission from the first nitrogen ion laser. The output beam is seen in the photograph striking the ruled translucent target in the lower left. The emission consists of a single spectral line of less than 0.3 nm linewidth at 427 nm in the violet. The laser cavity is contained in the pressure vessel with sapphire windows sealed across the optical axis. It is the most efficient visible laser constructed to date emitting 1.8% of the electron beam energy deposited in the gas.

I. TECHNICAL REPORT SUMMARY

It was recently proposed by Collins, et. al.[1] that resonant charge transfer reactions might provide nearly ideal pumping mechanisms for recovering one photon for each ion produced by the discharge of an intense electron beam into high pressure gases. Since the energy from an e-beam discharge can be stored at densities of the order of kilojoules per liter with efficiencies over 50%, such a pumping mechanism would clearly point toward the development of e-beam lasers operating at visible wavelengths with system efficiencies between 5 and 10%. The potential of the pumping reaction

$$He_2^+ + N_2 \rightarrow N_2^+ (B^2\Sigma_u^+) + 2He, \qquad (1)$$

was reported in the same letter, together with construction of a two-pass amplifier excited by a Febetron 706 and operating at 427.8, 470.9 and 522.8 nm.[1]

As reported subsequently at the VIII IQEC Conference, we have now successfully constructed the first nitrogen ion laser pumped by charge transfer from He_2^+. Intense laser emission at 427 nm has been produced with an efficiency of 1.8% relative to the energy lost by the electron beam in the radiating volume.

The laser device consisted of a pair of 1 m dielectric mirrors which were mounted to allow angular alignment, spaced with 14 cm invar rods, and contained in a stainless steel pressure vessel with sapphire windows sealed across the optical axis external to the cavity. In operation the system was pressurized with 7 atmospheres of a mixture of helium and nitrogen. Useful partial pressures of nitrogen ranged from 2 to 20 Torr. Excitation was provided by an electron beam entering through a supported, 0.002-in thick titanium foil window and propagating in a direction perpendicular to the optical axis. The cross

section of the beam was 1 cm x 10 cm with the longer transverse axis coincident with the optical axis of the cavity. The electron beam was emitted by APEX-1, pulsed at 14 KA and 950 KV for a duration of 20 nsec with rise and fall times of 7 nsec.

Spectra were recorded with an oscilloscope camera focused on the image plane of a 0.25 m Jarrell Ash spectrometer with the exit slit removed. Resolution was limited to 0.3 nm by the width of the entrance slit and the dispersion of the grating. The time dependence and power level of the light output was measured with a calibrated ITT F-4000, S20 vacuum photodiode connected directly to a Tektronix 519 oscilloscope. Proper attenuation of the laser output was provided by calibrated neutral density filters.

In operation intense laser emission was observed in the violet at 427 nm and found to have a linewidth less than 0.3 nm. Beam divergence was measured to be 20 milliradians from photographs of the illuminated spot on targets successively placed at distances varying from 1 to 10 m.

Examination of the spectrum of the laser emission showed the single line at 427 nm corresponding to the band head in the P-branch of the (0, 1) vibrational transition of the $B^2\Sigma_u^+ \rightarrow X^2\Sigma_g^+$ electronic transition of the nitrogen molecular ion, N_2^+.

The radiating volume was estimated to be 0.625 cm^3 from application of a double cone geometry to enlarged photographs of the illuminated spot at the base of the cone on the output dielectric mirror, and from this energy densities corresponding to the observed output could be calculated. A summary of output energy as a function of nitrogen partial pressure and cavity loss per round trip transit is shown in Table 1.

TABLE 1

Summary of nitrogen ion laser output at 427 nm for 7 atm of helium and various partial pressures of nitrogen.

N_2 Pressure (Torr)	Mirror Losses (%/roundtrip)	Pulse Width (nsec)	Energy Density (Joules/liter)
2.2	19	6	.003
2.2	11.8	10	.010
2.2	8.8	14.2	.038
5.1	8.8	15.8	.208
10	8.8	15	.218
20	8.8	11	.085

In the case of the first entry in Table 1, the larger mirror losses prevented lasing until later in the afterglow period. This was seen as a pronounced displacement of the output pulse to later time. This placed a lower limit on the small signal gain of 0.01 cm^{-1} averaged over the 20 cm path length for a round trip transit.

Under the more nearly optimal combination of pressure and cavity losses the decay of the pulse was seen to correspond to the ringing down time of the cavity and indicated that the total energy of the output pulse was extracted prior to the pulse maximum at 11 nsec. The energy lost by the beam during the corresponding first 11 nsec can be calculated from range-energy consideration to be 12.4 J/liter. This gives an output efficiency for 427 nm radiation of 1.8% relative to beam energy lost in the radiating volume. This is to be compared with the theoretical limit of 6.8% for delta function, e-beam excitation at a time early enough for reaction (1) to go to completion. Elementary considerations indicate that, with the proper mirror sets, similar efficiencies can be

obtained from parallel transitions in this system at 471 nm in the blue and possibly at 523 nm in the green, and current analysis of kinetic loss mechanisms suggests that with proper optimization the theoretical limit on efficiency of 6.8% can be approached.

Details of the experimental achievements to date are summarized in the manuscript, "A Nitrogen Ion Laser Pumped by Charge Transfer", by C. B. Collins, A. J. Cunningham, and M. Stockton, which has been accepted by Applied Physics Letters. A full presentation of the results currently available is contained in the following material.

The promise of the nitrogen ion laser is clearly of such importance that substantial continuing effort to optimize its performance is warranted. However, it must be realized that it is only the first example of the new class of e-beam lasers pumped by charge transfer[1] and other similar systems offer the possibilities of even higher efficiencies and broader selections of output wavelengths. Nevertheless, the high efficiency already observed for the emission of 427 nm laser radiation from this system points to the nitrogen ion laser as a device of considerable significance and clearly confirms the importance of charge transfer reactions as laser pumping mechanisms.

II. THEORETICAL MODEL

The development of intense pulsed electron beam sources in the 1 to 100 Gigawatt class have made feasible the deposition of energy in the form of ionization into large volumes of plasma with system efficiencies around 50%. Given an elementary mechanism utilizing this ionization and leading to the inversion of population at quantum efficiencies which are typically 10 to 20%, overall radiative efficiencies of the order of 5 to 10% can be realistically projected, provided the plasma constituents are arranged to allow for the domination of the desired reaction channel. The xenon excimer laser[2,3] is the best example of such a system in which the primary mechanism is the dissociative recombination of the Xe_2^+ ion. Though superficially similar, the electron beam excited N_2[4] and H_2[5] lasers do not actually utilize the primary ionization of the plasma; consequently, system efficiencies are reduced by orders of magnitude.

Evidently, charge transfer between the population of primary ions and a minority constituent of lower ionization potential offers a nearly ideal mechanism[1] for ultimately obtaining one photon per primary ion. If the minority constituent is selected to have the energy of an excited state of its ion approximately equal to that of the primary ion, in principle, one photon per ion can be realized with a quantum efficiency, E, equal to

$$E = \frac{IP(1)-IP(2)}{IP(1)} \qquad (2)$$

where IP(1) and IP(2) are the ionization potentials of the primary and secondary constituent, respectively. Table 2 summarizes examples of possible system efficiencies characteristic of various permanent gases diluted in helium.

TABLE 2

Projected system efficiencies for the emission of radiation following charge transfer excitation from the helium molecular ion, assuming a 50% efficiency for the production of ionization by electron beam impact.

Minor Constituent	Overall Efficiency
N_2	11.0%
O_2	12.5%*
CO	14.5%

*The resonant transition does not terminate on the ground state of the molecular ion.

Similar possibilities occur with other primary species, but at efficiencies reduced by the lower ionization potential of those species.

Both the available output energy and pulse duration depend strongly on partial pressures, and the high values of charge density which become feasible with e-beam excitation are needed. The deposition of energy into a high pressure gas by an electron beam is a very complex problem, and most characterizations of the process have been made for the excitation of dense inert gases. In such systems as xenon, beam-plasma effects rapidly dominate with the return currents[6,7] playing a large role. However, in the singular case of the light inert gases at beam currents below 20 KA, simplifying assumptions exist which render the problem tractable. Subject to limitations on the product of gas density and beam penetration depth, to be discussed below, the problem can be resolved into that of the differential energy loss in the gas of β-particles in a beam, the morphology of which is completely determined by the foil window through which the beam has entered.

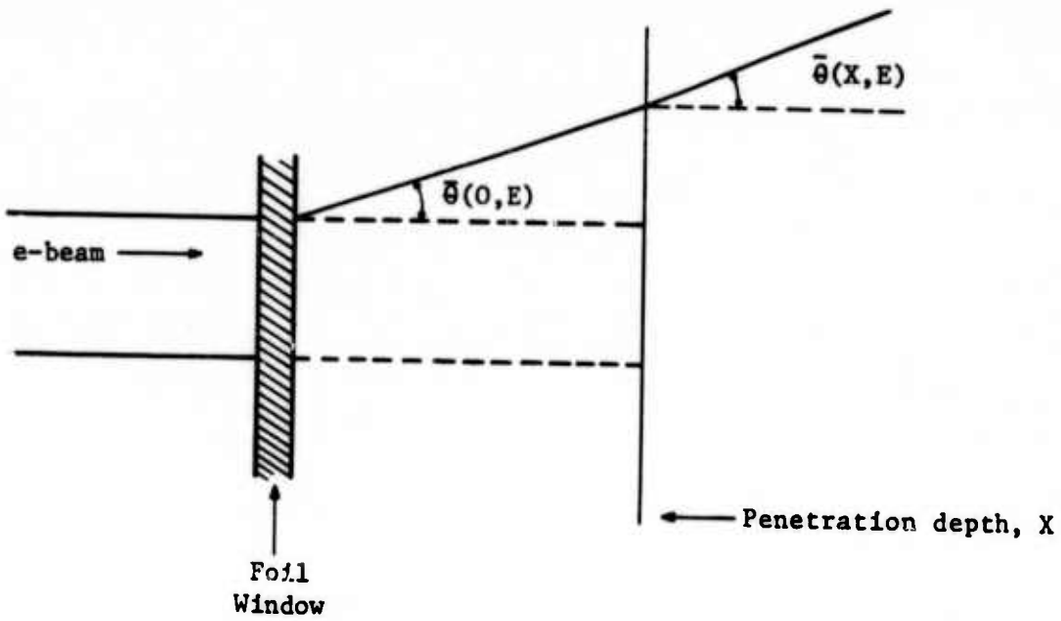

Figure 1: Schematic drawing of electron beam injection into high pressure gas sample.

Referring to Fig. 1, the mean scattering angle $\bar{\theta}(E)$ of electrons exiting from the foil window can be readily calculated for the case of "multiple scattering,"[8] which corresponds to that descriptive of foils of realistic dimensions. After some distance of penetration, X, into the gas, the mean scattering angle has increased to a value $\bar{\theta}(X,E)$. To determine the conditions under which $\theta(X,E)$ differs significantly from $\bar{\theta}(0,E)$, assume

$$\bar{\theta}(X_E,E) \geq 1.1\ \bar{\theta}(0,E) \quad , \tag{3}$$

or that at the critical depth of penetration, X_E, for that energy, E, the root-mean-square scattering angle is increased 10%. Since angles of magnitude $\bar{\theta}(0,E)$ are characteristic of multiple scattering conditions, it is reasonable and consistent to assume those of $\bar{\theta}(X_E,E)$ are similarly characteristic. Expressions for $\bar{\theta}(X,E)$ are tedious though well-established[8] and substitution into (3) yields for a titanium foil, .002" thick, after simplification

$$\frac{90.66}{Z\sqrt{B}} \geq \sqrt{PX_E} \qquad (4)$$

where P is the gas pressure in atmospheres, Z, the atomic number and B a scattering constant related to, n, the probable number of collisions in the scattering layer of thickness X_E. To within 10%, explicit dependence of (3) on beam energy can be cancelled for E ≤ 1MeV, as was done in the simplifications yielding (4), and the remaining critical parameters X_E and P depend on E only through B. By choosing the energy E ≤ 1 MeV making (4) its most restrictive, X_E can be replaced by X. Considering two cases, helium and argon, B can be written as follows:

$$\text{for } Z = 2 \quad B \tilde{=} .43 + 2.93^{10}\log PX, \qquad (5a)$$

$$\text{for } Z = 18 \quad B \tilde{=} 3.97 + 2.93^{10}\log PX, \qquad (5b)$$

where units are as in (4). Then substituting into (4) and solving for the roots of the resulting transcendental equation give the limits on negligible scattering in the region adjacent to a titanium foil of .002 inch thickness,

$$PX \text{ (Helium)} \leq 273 \text{ atm. cm} \tag{6a}$$

$$PX \text{ (Argon)} \leq 4.3 \text{ atm. cm} \quad . \tag{6b}$$

It can be seen from these results that, whereas the simplifying assumptions break down for argon (Z=18) at an inch of penetration at two atmospheres, they remain valid in helium (Z=2) over the entire span of parameters required for practical operation of a small test laser device. For example, at 30 atmospheres pressure, the simplified model is valid to at least 9.10 cm depth of penetration which is sufficient to describe about a half liter volume excited by a 1 x 10 cm electron beam of divergence characteristic of transmission through a .002" titanium foil window at 1 MeV for currents less than 20 KA. At higher currents, the "drag e.m.f."[7] resulting from the return currents should be considered.

In the following material the theoretical model derived will be understood to be subject to the restrictions

$$E \leq 1 \text{ MeV} \tag{7a}$$

$$I_o \leq 20 \text{ KA} \tag{7b}$$

$$PX \leq 280 \text{ atm. cm} \tag{7c}$$

and the beam input to the foil window will be assumed to have a 1 x 10 cm transverse cross-section.

Since it will now be assumed that the beam propagation in the high pressure gas has been determined by the scattering in the foil window, an examination of the resulting beam divergence is necessary. For the conditions of multiple scattering which apply in the most practical conditions considered here, the distribution of scattering angles is given by the expression[8]

$$dP = P(\theta)2\Pi\theta d\theta = 2e^{-(\alpha\theta)^2}\alpha\theta\, d(\alpha\theta)\ , \qquad (8)$$

where $\alpha = \bar{\theta}^{-1}$ is the inverse of the most probable scattering angle and P the probability of finding the incident electron scattered into the conical shell lying between polar angles θ, and $\theta+d\theta$ as in Fig. 1. What is needed is the most probable path length of an electron emerging from the foil per centimeter of penetration depth X, measured normal to the window foil. The infinity in path implied by 90^{o} scattering can be compensated by "cutting-off" the integral at the particular angle θ_c where

$$\theta_c(X) = \text{arc tan } Xo/r \qquad (9)$$

and where r is the radius of the walls of the confining pressure chamber and Xo is the minimum penetration depth which can be sampled. In practice, the finite thickness of the mechanical components used to retain the foil effectively "block" any transverse optical paths lying closer to the foil than Xo = 0.5cm. In this case, a practical path average is

$$(X-Xo)\int_0^{\theta_c} dP \quad \langle(\cos\theta)^{-1}\rangle = (X-Xo)\int_0^{\theta_1}(\cos\theta)^{-1}dP$$

$$+\int_{\theta_1}^{\theta_c}\left(\frac{r}{\sin\theta} - \frac{Xo}{\cos\theta}\right) dP \qquad (10)$$

where now θ_1 = arc cot X/r is the angle at which the path strikes the wall of the confining chamber before penetrating a depth X. The resulting expressions can be approximated to within 10% to involve only the exponential integrals $E_i(y)$ where

$$y = \left(\frac{\pi}{2}\alpha\right)^2,\ \left(\frac{\pi}{2}\alpha\right)^2\left(1-\left(\frac{2\theta_1}{\pi}\right)^2\right),\ \text{and}\ \left(\frac{\pi}{2}\alpha\right)^2\left(1-\left(\frac{2\theta_c}{\pi}\right)^2\right),$$

and

$$E_i(y) = \int_{-\infty}^{y} \frac{e^x}{x}\,dx \quad . \tag{11}$$

Fig. 2 presents the solutions for the mean path length in terms of the angle

$$\bar{\psi} = \arccos\left[\langle(\cos\theta)^{-1}\rangle\right]^{-1} \quad , \tag{12}$$

the angle at which the electron traverses a path of average length as given by (10) in penetrating to a depth X. Notice that $\bar{\psi} \neq \bar{\theta}$ for either of the two depths of penetration shown. However, for large $\bar{\theta}$, the scattering is more probably described by diffusion[8] of the electron beam through the foil and in the saturated diffusion limit

$$dP_s \propto (.717+\cos\theta)\cos\theta\sin\theta d\theta \ , \tag{13}$$

and the analogous relation to (10) is

$$\langle(\cos\theta)^{-1}\rangle \int_0^{\pi/2} dP_s = \int_0^{\pi/2} (\cos\theta)^{-1} dP_s \ , \tag{14}$$

giving

$$\bar{\psi}_s = 45.17^\circ \quad , \tag{15}$$

where the subscripted s refers to the saturated distribution. This limit is shown in Fig. 2 as the dashed limit and, in fact, must represent an asymptote to $\bar{\psi}$ as a

Figure 2

Graph of mean path angle, $\bar{\psi}$, defined in eq. (12) as a function of the mean scattering angle, $\bar{\theta}$, defined in eq. (8).

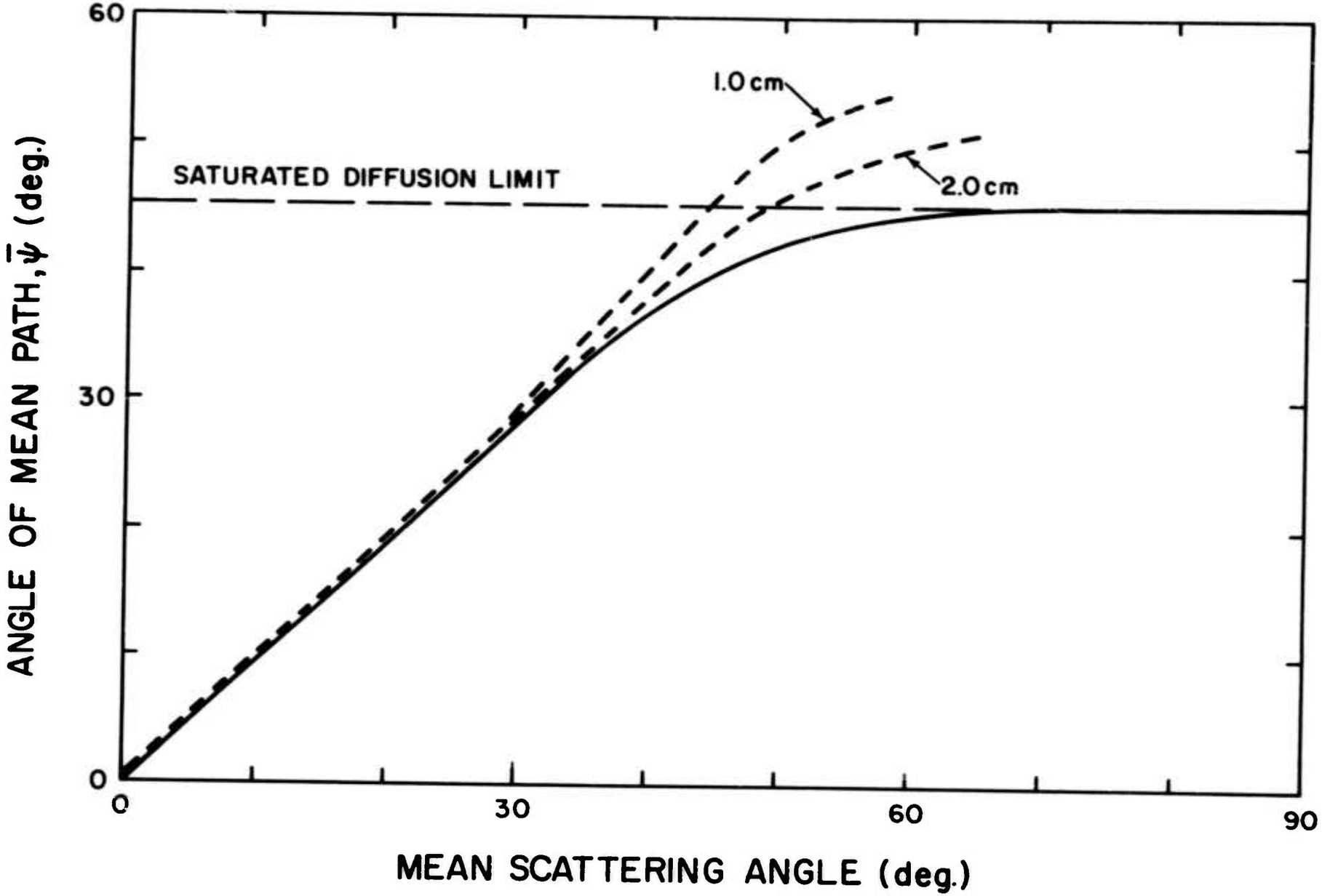
60
30
0
0
30
60
90
1.0 cm
2.0 cm
SATURATED DIFFUSION LIMIT
ANGLE OF MEAN PATH, $\bar{\psi}$ (deg.)
MEAN SCATTERING ANGLE (deg.)

function of $\bar{\theta}$. However, as $\bar{\theta}$ increases, the type of scattering passes from "multiple" to saturated diffusion and at larger $\bar{\theta}$, expression (10) does not correctly account for the angular distribution of the scattered beam preventing this asymptote being attained. As the intermediate case of scattering is quite difficult to treat exactly, the graphical interpolation shown by the heavy solid curve of Fig. 2 was constructed for use in the theoretical model. In practice the transition region between 40° and 60° corresponds to the energy range of 0.5 to 0.3 MeV for a .002" thick titanium foil and so is of significance for a relatively small interval of time on the leading and the trailing edge of the e-beam pulse. This, coupled with the small difference in the $\bar{\psi}$'s obtained from the two models of large angle scattering, limits errors resulting from the use of the graphical interpolation to a few percent.

To determine the scattering angle as a function of beam energy, the functional dependence of $\bar{\theta}$ on E must be determined. Defining

$$\bar{\theta} = X_c\sqrt{B} \quad , \tag{16}$$

where for a foil .002 inches thick

$$X_c = 10.99\ (E)^{-1}\left[\frac{1 + 1.957E}{2 + 1.957E}\right]\ \text{(degrees)} \quad , \tag{17}$$

E is in MeV, and B is the scattering constant involved in (4) which in the case of titanium is best determined from the tabulation of Ref. 8. The variation in B over the appropriate range, from 0.2 to 1.0 MeV, is only 7.9 to 7.3. Then, calculating $\bar{\theta}$ from (16) and (17) and using Fig. 2 to determine $\bar{\psi}$ gives the functional dependence on E shown in Fig. 3. Also shown is the attenuation of the beam current, relatively small for titanium, resulting from back diffusion of the beam electrons. The attenuation of beam energy is of much greater significance and is considered next.

Figure 3

Graphs of mean path angle, $\bar{\psi}$, and beam attenuation as functions of e-beam energy input to the .002" thick Ti foil. The ordinate scale is common to both graphs and units for each are shown in parentheses.

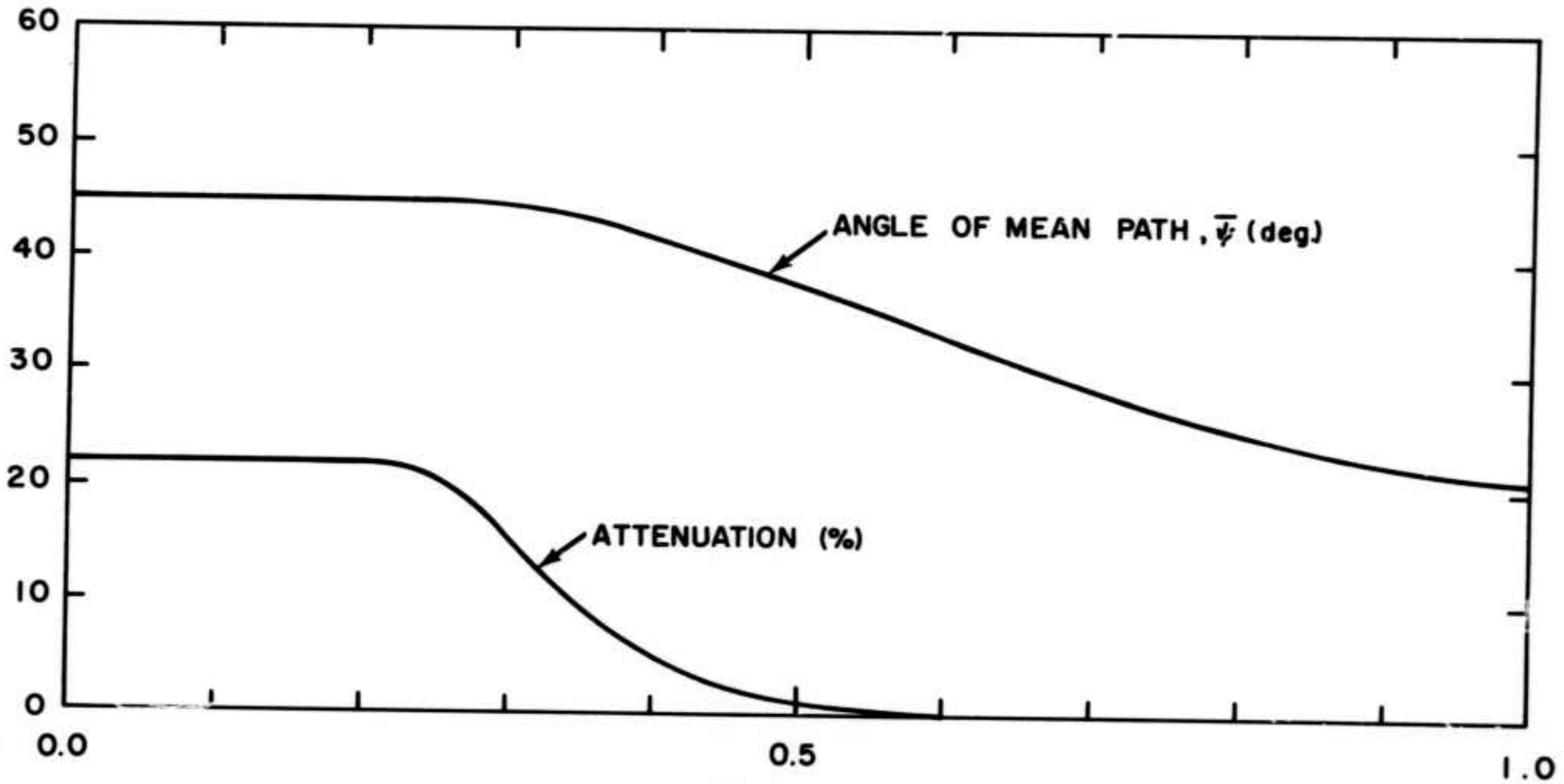
60
50
40
30
20
10
0
0.0
0.5
1.0
ANGLE OF MEAN PATH, $\bar{\psi}$ (deg.)
ATTENUATION (%)
INPUT E-BEAM ENERGY (MeV)

At relativistic energies, the beam energy lost in the foil can be expressed simply as the Bethe-Block expression for the differential energy loss multiplied by the mean path length in the foil. For titanium foil, this expression takes the form

$$-\frac{dE}{dx} = 0.3156\beta^{-2}\ [15.48 + \ln(1+1.957E)^2\beta^2E + (1-\beta^2)$$

$$-(2\sqrt{1-\beta^2}-1+\beta^2)\ln 2 + 1/8(1-\sqrt{1-\beta^2})^2\ ] \quad (\text{MeV/cm}) \quad , \qquad (18)$$

where $\beta = v/c$ and the energy loss ΔE is

$$\Delta E = (-\frac{dE}{dx})\frac{\Delta X}{\cos\bar{\psi}} \quad , \qquad (19)$$

where ΔX is, in this case, the foil thickness. At lower energies, $\beta < 0.5$, ΔE can become a significant fraction of the beam energy and the non-relativistic expression for the differential energy loss must be used,

$$-\frac{dE}{dx} = .6311\ \beta^{-2}\ \ln(5272.7E). \qquad (20)$$

The quantity desired is the energy of the beam emerging from the foil as a function of the input energy so (20) must be integrated in the form

$$\int_{E_o}^{E(x)} \frac{dE}{f(E)} = (\cos\bar{\psi}(E_o))^{-1} \int_o^x dx \quad , \qquad (21)$$

and the resulting expression for E(x) solved in terms of E_o. Equation (21) can be expanded into the series

$$C^{-1}\sum_{n=2} (-1)^n\, n\, (aC^{-1})^{n-1} \int_{n\ln(CE(x))}^{n\ln(CE_o)} \frac{e^z}{z}\, dz = Kx(\cos\bar{\psi})^{-1} \quad , \qquad (22)$$

where C = 5272.7, K = .6311, and a = 1.957. For a given foil thickness R, as the input beam energy decreases, E(R) decreases until zero is reached at which time that thickness, R, corresponds to the range of the electrons of that energy, E_o. Lower energy electrons will not penetrate the foils, and the characteristic transmission of the foil shows a sharp onset at that energy E_o, for which its range is equal to the foil thickness. To within two percent equation (22) can be re-written in terms of the range $R(E_o)$ corresponding to a given input beam energy as

$$\frac{1}{a\ln(CE(x))}\left[(1+aE(x))^{-1} - (1-aE(x)) + \frac{1}{\ln(CE(x))}\left\{aE(x)-\ln(1+aE(x))\right\}\right]$$

$$= \frac{K[R(E_o)-x]}{\cos\bar{\psi}} \qquad (23)$$

The roots of this expression give the energy of the emerging beam, E(x), in terms of the energy of the input beam, E_o, and the range $R(E_o)$ of those electrons in the foil. It is that energy which is then characteristic of the beam injected into the high pressure gas.

The energy deposited in the gas can be approximated by the expression

$$\Delta E = \left(-\frac{dE}{dx}\right) \Delta X\, (\cos\bar{\psi})^{-1} \quad , \qquad (24)$$

since, in this case, the range of energies over which $\Delta E \sim E(x)$ is much smaller in these relatively thin gas samples. At low beam energies in helium,

$$(-\frac{dE}{dx}) = 27.3\ P\beta^{-2}\ [10.380 + \ln E]\ (\text{volts/cm})\ , \qquad (25)$$

for $\beta < 0.5$ and

$$(-\frac{dE}{dx}) = 13.65\ P\beta^{-2}[19.10 + \ln\ (1+1.957E)^2\ \beta^2 E$$

$$+ (1-\beta^2) + (2\sqrt{1-\beta^2})\ \ln 2 + 1/8\ (1-\sqrt{1-\beta^2})^2\ ]$$

$$(\text{volts/cm})\ , \qquad (26)$$

where P is the pressure in atmospheres.

Combining now the data calculated for $\bar{\psi}$ as a function of E_o from Fig. 3, the roots of E(x) as a function of E_o from (23), and $(-\frac{dE}{dx})$ from (25) and (26) according to (24) gives differential energy loss per unit penetration depth as a function of electron beam energy input to the .002 inch thick foil window of an experimental device. Values of this function are plotted in Fig. 4 in units of KV/atm/cm for various input e-beam energies. Over a small range of E_o, ΔE computed according to (24) exceeded the energy E(x) of the emerging beam. For those values of E_o, E was replaced by E(x) in accordance with the assumption that all the energy of the emerging beam is stopped in the experimental volume bounded by the penetration depth ΔX.

The spike seen in Fig. 4 corresponds to those conditions for which most of the beam energy is deposited in the foil and the beam emerges at low velocity giving a relatively large (-dE/dx). However, since in the cases considered here the beam spends relatively little time at those energies, the total ionization resulting from those conditions is small.

The power deposition per unit volume can be written by considering that the energy lost by the beam in penetrating to a depth X is deposited in a rectangular pyramid with its sides slanting with angle $\bar{\psi}$ away from the beam axis,

Figure 4

Graph showing the differential energy loss per unit penetration depth in helium in units KV/cm/atm as a function of electron beam energy input to a 0.002 inch thick Ti foil window of the experimental device.

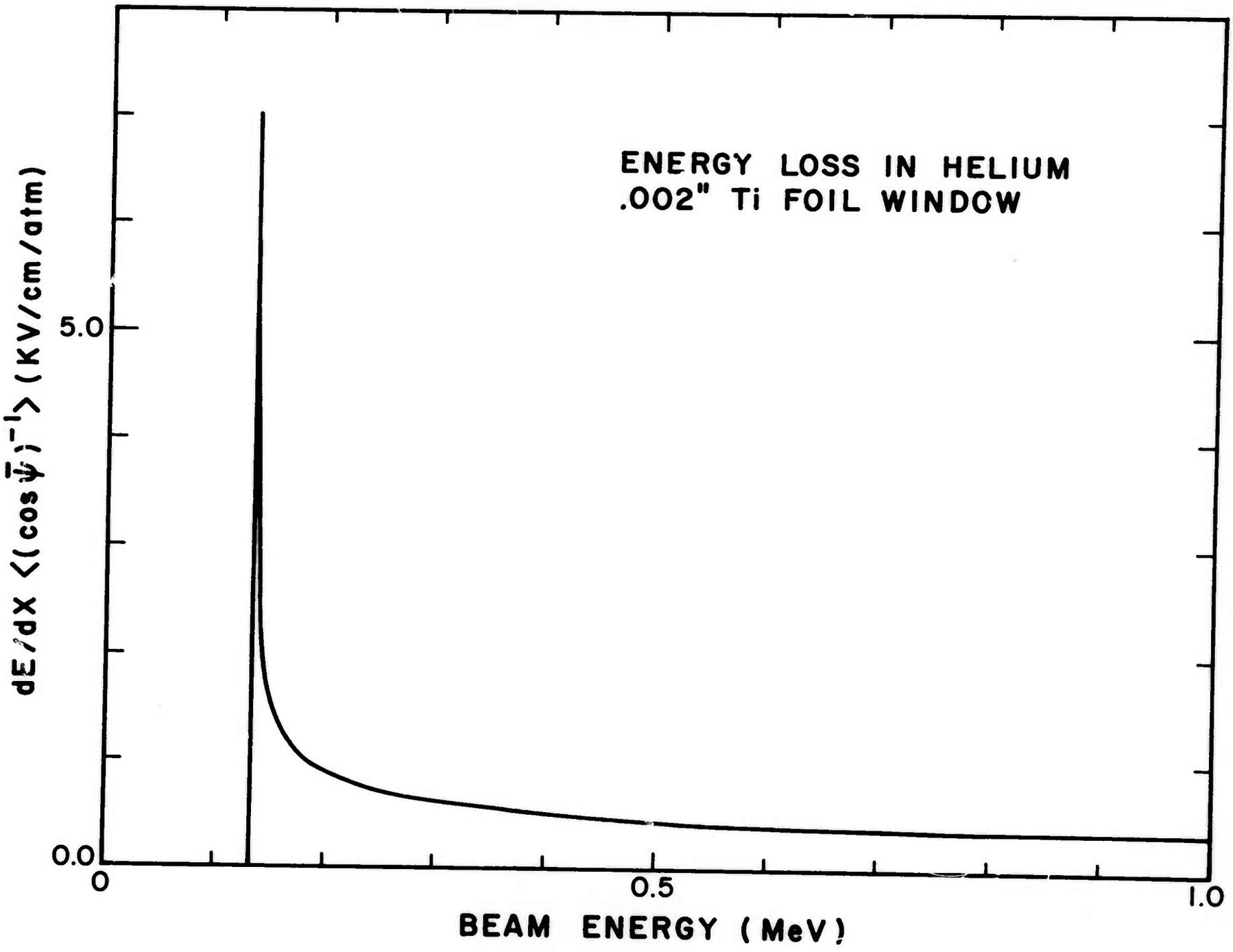
ENERGY LOSS IN HELIUM
.002" Ti FOIL WINDOW
dE/dX <(cos ψ)^-1> (KV/cm/atm)
5.0
0.0
0
0.5
1.0
BEAM ENERGY (MeV)

truncated at the foil surface and having its base on the plane located a distance X from the foil and normal to the beam axis. The volume of such a figure is

$$\Delta V = X\,[10 + X\,(11 \tan \bar{\psi} + 4/3 \tan^2 \bar{\psi})] \quad , \tag{27}$$

and depends on beam energy, E_o, through $\bar{\psi}$. Then the energy deposition can be written

$$d\varepsilon\,(X,E_o) = \frac{I_o\,(t)\,[1\text{-Att}\,(E_o)]}{10 + [11 \tan \bar{\psi}\,(E_o) + 4/3 \tan^2 \bar{\psi}\,(E_o)]X} \cdot$$

$$\left\{ - \frac{dE}{dx}\,(E_o)\,(\cos\bar{\psi}(E_o))^{-1} \right\} dt \quad , \tag{28}$$

where the term in braces is that shown in Fig. 4 and 1-Att can be obtained from Fig. 3. The beam current $I_o(t)$ can be written in terms of $E_o(t)$ and a constant Ω, by assuming

$$I_o(t) = \frac{1}{\Omega}\,E_o\,(t) \quad . \tag{29}$$

Further assuming the beam energy has a time dependence,

$$E_o(t) = \begin{cases} (t/\tau)\ \text{MeV} & \text{for } t \leq \tau \\ 1\ \text{MeV} & \text{for } t > \tau \end{cases} \quad , \tag{30}$$

and $dt = \tau dE$ where E is in MeV and $t \leq \tau$. Then the energy deposited in the experimental volume, ΔV by the time t is

$$\varepsilon\,(t) = \int_o^t d\varepsilon \tag{31}$$

which can be written in terms of an ionizing function

$$F(E) = E \frac{[1-Att]}{\left(\frac{\Delta V(E,X)}{X}\right)} \left[- \frac{dE}{dx} (E) . (\cos \bar{\psi}(E))^{-1} \right] , \quad (32)$$

as

$$\varepsilon(t) = \int_0^E F(E')\, dE' = \frac{\tau_N}{\Omega} \int_0^E F(E') dE' \text{ (Joules/}\ell\text{/atm)}, \quad (33)$$

where τ_N is the risetime τ in nanoseconds and Ω is now 1 MeV/I_o where I_o is the maximum beam current in amps. F(E) is plotted for helium for the case X=2cm in Fig. 5 and serves as a model for obtaining the energy expended by the time the beam energy has risen to a value E_o following initiation of the e-beam discharge. For times $t > \tau$ the beam energy is constant, as is the power deposition, and $d\varepsilon$ becomes

$$d\varepsilon = \frac{126}{\Omega} \text{(Joules/}\ell\text{/nsec)} , \quad (34)$$

The cumulative energy deposition can then be calculated, once the time dependence of the input e-beam is known, by integrating the deposition function of Fig. 5 for $t < \tau$. For times greater than τ, the value of

$$\int_0^\tau d\varepsilon = 8.65\, \tau_N/\Omega \text{ (J/}\ell\text{/atm)} , \quad (35)$$

can be used to describe the total deposition on the leading edge of the pulse. Then to $t = T_N$, the time bounding the end of the plateau (in nanoseconds),

Figure 5

Logarithmic graph of ionizing function, F(E) defined in eq. (32) for helium as a function of e-beam energy input to the .002" thick Ti foil. The integral of this curve multiplied by τ_N/Ω give the energy deposition in Joules/liter/atm.

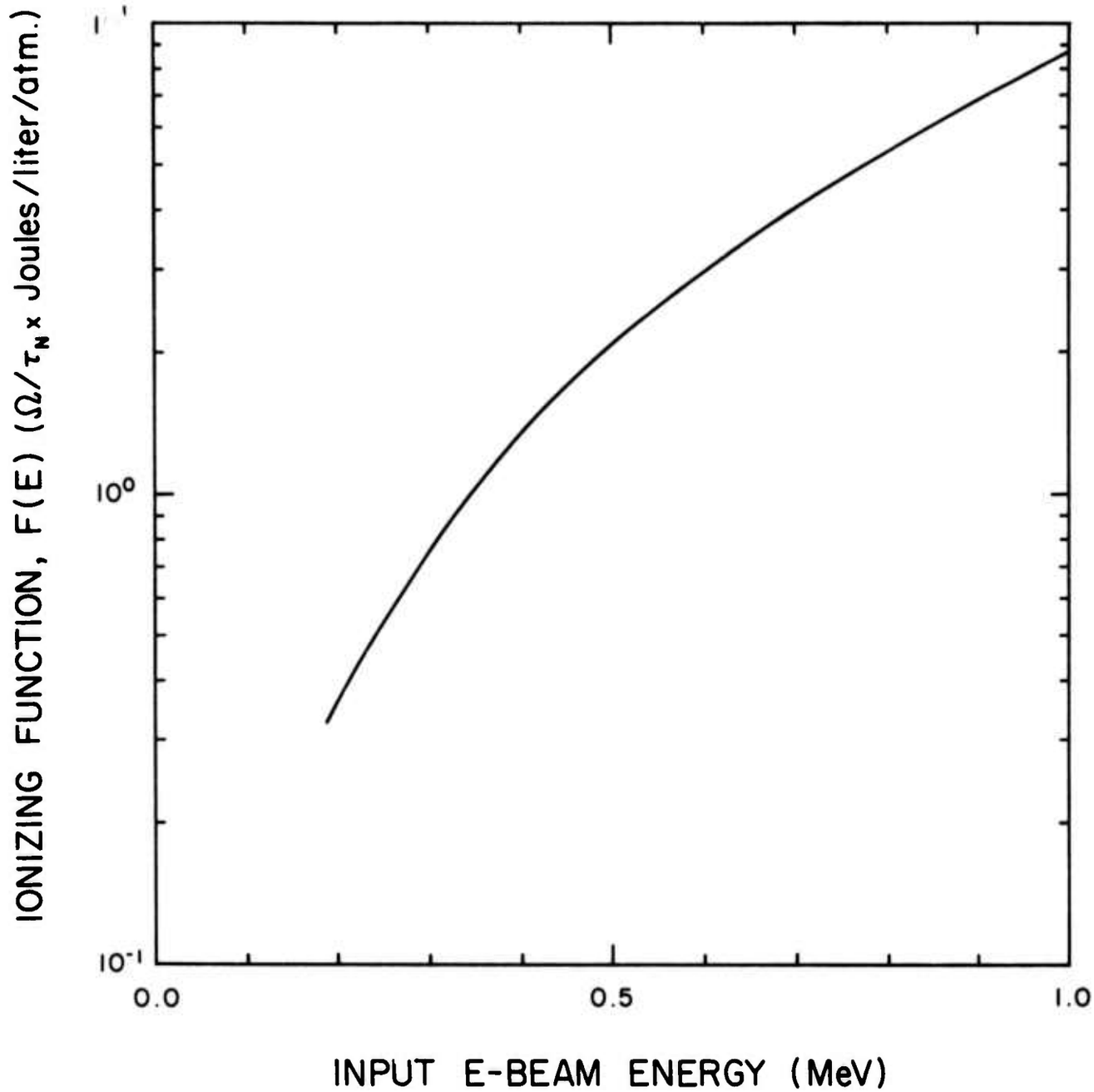
IONIZING FUNCTION, F(E) (Ω/τ_N x Joules/liter/atm.)
10^1
10^0
10^{-1}
0.0
0.5
1.0
INPUT E-BEAM ENERGY (MeV)

$$\varepsilon(t) = 8.65\ \tau_N/\Omega + 18.05\ (T_N - \tau_N)/\Omega \text{ (Joules/}\ell\text{/atm)}, \quad (36)$$

provides a reasonable model. Finally considering, for simplicity, the tail of the pulse to be a linear decay similar to the leading edge,

$$\varepsilon = 17.3\ \tau_N/\Omega + 18.05\ (T_N - \tau_N)/\Omega \text{ (Joules/}\ell\text{/atm)}. \quad (37)$$

For APEX-1, the electron beam device used in these experiments,

$$\tau_N = 6.6 \text{ nsec}, \quad (38a)$$

$$T_N = 20 \text{ nsec}, \quad (38b)$$

and Ω^{-1} can be written for a 1 MeV maximum output

$$\Omega^{-1}/I = 10^{-3}\ (\text{KA})^{-1} \quad . \quad (38c)$$

Then

$$\varepsilon = 0.356 \text{ Joules/}\ell\text{/atm/KA} \quad . \quad (39)$$

This can be related to the ionization produced by recognizing that the energy cost per ion in helium[9] is 42.3 eV and that 1 Joule/ℓ will produce 1.478×10^{14} ions/cm^3. The energy stored as ionization is 24.5 eV per ion so that the efficiency of energy storage is

$$\text{Eff} = 57.9\% \quad . \quad (40)$$

Table 3 summarizes the energy storage which can be achieved in helium excited by APEX-1, a 100 KA, 1 MeV, e-beam device pulsed typically for 20 nsec FWHM with 6.6 nanosecond rise and fall times.

TABLE 3

Summary of the energy density stored as ionization in high pressure helium following discharge of APEX-1. The efficiency of the storage relative to the total energy deposited by the beam is 57.9%.

	ENERGY DENSITY (JOULES/LITER)	
Beam Current	20 KA	100 KA
Pressure		
3 atm	12.4	62
30 atm	124	620

The ionization produced can be obtained from Table 3 by noting that 1 Joule/ℓ stored as He^+ represents 2.55×10^{14} ions/cm^{-3}. According to (40), an elementary mechanism utilizing this ionization and leading to the inversion of population would make possible overall radiative efficiencies about half of the absolute quantum efficiency of the transition. In the visible wavelength region, this would mean efficiencies between 5 and 10%, provided the plasma constituents could be arranged to allow for the domination of the desired reaction channel.

Evidently, a resonant charge transfer reaction between the population of primary ions in the plasma and a minority constituent of lower ionization potential offers a nearly ideal mechanism for ultimately obtaining one photon per primary ion. Fig. 6 presents the energy level diagrams of the ions of helium and nitrogen. Studies[10] on low pressure charge transfer mixtures have shown the strong development of spectra from molecular ion levels in near resonance with the primary helium ions. One such selectively excited transition is indicated by the arrow in Fig. 6. Particular charge transfer reactions are of the form

$$He^+ + XY \rightarrow (XY^+)^* + He \qquad (41a)$$

$$\rightarrow X^+ + Y + He \qquad (41b)$$

and

$$He_2^+ + XY \rightarrow (XY^+)^* + 2He \qquad (42)$$

where the asterisk indicates additional electronic excitation. Although quantum efficiencies are more favorable for reactions excited by He^+, in practice the importance of channel (41b) in the case of N_2 minimizes the importance of the He^+ ion.

At sufficiently high pressure, the He^+ is rapidly converted to He_2^+ by the termolecular reaction

Figure 6

Energy level diagrams for the ionic states of helium and molecular nitrogen.

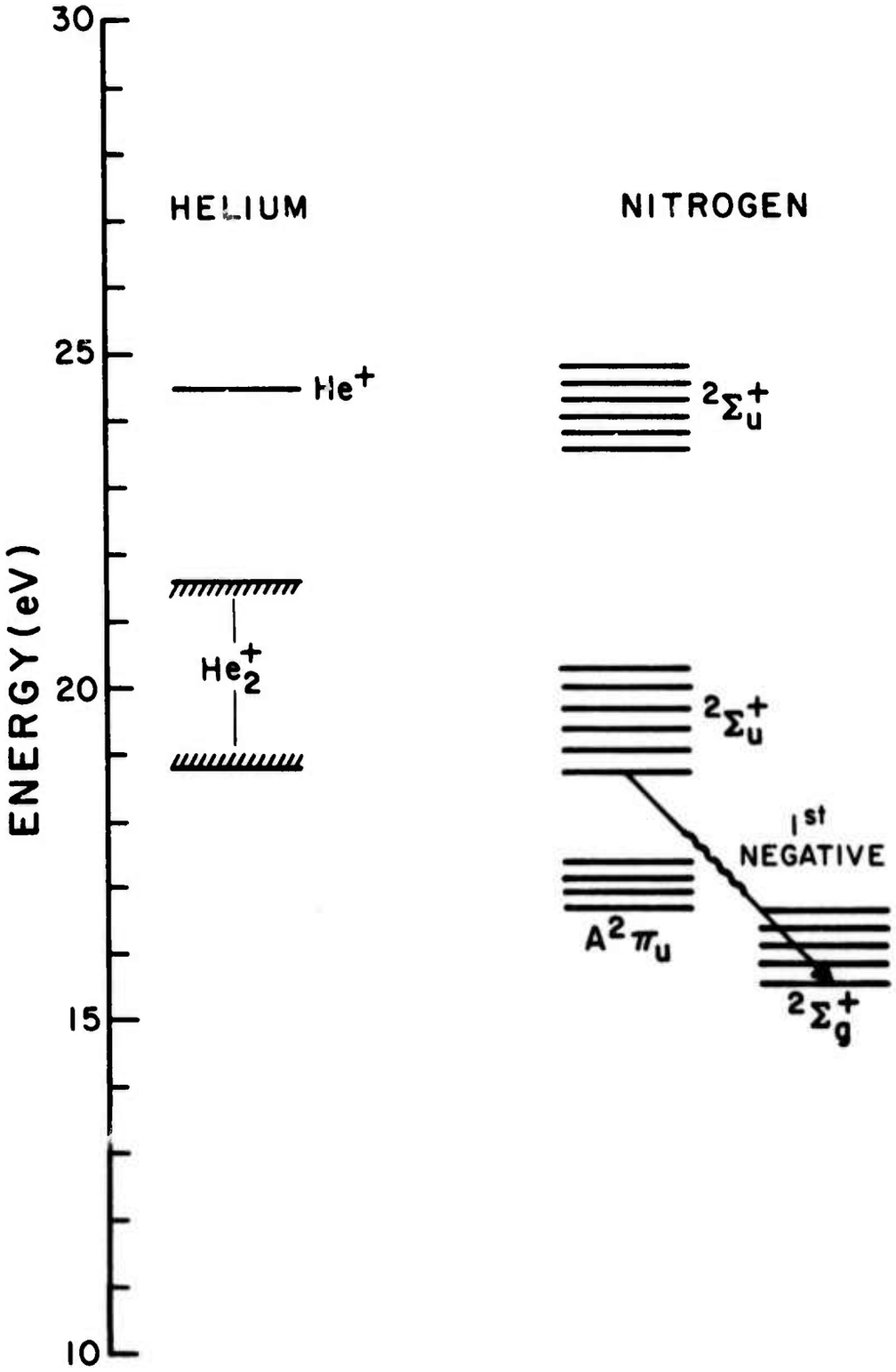
30
25
20
15
10
ENERGY (eV)
HELIUM
NITROGEN
He+
He2+
2Σu+
2Σu+
1st
NEGATIVE
A2πu
2Σg+

$$He^+ + 2He \rightarrow He_2^+ + He \tag{43}$$

with a characteristic lifetime of

$$\tau = \frac{27}{p^2} \text{ nsec}^{11} \tag{44}$$

where p is in atmospheres. Provided the partial pressure of minority constituent is not too great for reaction (43) to go to completion, the ionization will convert from He^+ to He_2^+, thus making available the charge transfer reaction

$$He_2^+ + N_2 \rightarrow (N_2^+)^* + 2He \quad . \tag{45}$$

This reaction[12] has a rate coefficient of about 10^{-9} cm^3 sec^{-1} as does the analogous reaction[12] with He^+.

Requiring, then, a low enough partial pressure of minority gas so that reaction (43) can reach an $(1-e^{-1})$ end-point yield in competition with the competing channel for the loss of He^+ through unwanted charge transfer sets the upper limits on the partial pressures shown in Table 4.

TABLE 4

Partial pressures of He and diatomic admixtures to allow for a conversion of a fraction of $(1-e^{-1})$ of He^+ to He_2^+ in competition with charge transfer of He^+ and the resulting charge transfer lifetimes.

He	Max Admixture	Charge Transfer Lifetimes
3 atm	5.9 Torr	5.3 nsec
30 atm	590 Torr	0.05 nsec

Assuming that the lifetime of the source term for the minority excited states limits the rate at which energy can be extracted from the plasma through a stimulated transition, the minimum pulse widths can be computed from the partial pressures and these are shown in Table 4 above.

Referring back to Fig. 6, the probable wavelength and, hence, overall efficiency can be estimated. Both from a resonance argument and from prior observations[10] on lower pressure mixtures, the probable reaction products from (45) can be identified as $N_2^+(B^2\Sigma_u^+)$. The most probable transition is the (0,1) vibrational component of the $B \rightarrow X$ transition at 4278 Å. This corresponds to a 2.90 eV photon or an equivalent absolute quantum efficiency relative to the He^+ ion at 24.5 eV of 11.8%. This value together with expression (40) for the efficiency for the production of He^+ gives an overall efficiency Eff(λ) of

$$\text{Eff. } (4278\ \text{Å}) = 6.8\% \quad , \tag{46}$$

assuming reaction (43) goes to completion so that one photon per ion is realized.

From the above considerations, it appears peak power densities of the order of a Gigawatt per liter should be available to potential laser transitions for reasonable values of experimental parameters, provided the requisite population inversions occur. Considering only the better known N_2^+ system, the Einstein B-coefficient for absorption and stimulated emission can be written[14] as

$$B = \frac{1}{8\pi hc\nu^3} \quad \frac{g_n}{g_m} \quad \frac{1}{\tau} \tag{47}$$

where it is assumed the upper state is n and the lower, m; ν is in cm^{-1} and the g's are degeneracies, and for the $N_2^+(^2\Sigma_u^+ \rightarrow {}^2\Sigma_g^+)$, τ, the lifetime for spontaneous emission, is[15]

$$\tau = 66\ \text{nsec} \quad . \tag{48}$$

The expression for the amplification or absorption of radiation for an optical path length Δx in these units is [14]

$$\Delta I = I_o \cdot \Delta x \frac{Bh\nu}{\Delta\nu} \quad \frac{g_m}{g_n} \quad N_n \left(1 - \frac{g_n}{g_m} \frac{N_m}{N_n}\right) \quad , \tag{49}$$

where ΔI is positive for amplification, Δν is the bandwidth of the initial radiation, and I_o and ΔI are the intensity and intensity increment, respectively.

Substituting (47) into (49) gives

$$\Delta I = I_o \cdot \Delta x \frac{\lambda^2}{8\pi c \Delta\nu} \frac{1}{\tau} N_n \left(1 - \frac{g_n}{g_m}\frac{N_m}{N_n}\right) \quad . \tag{50}$$

The gain coefficient, κ, can be identified by inspection as

$$\kappa = \frac{\lambda^2}{8\pi c \Delta\nu} \frac{1}{\tau} N_n \left(1 - \frac{g_n}{g_m}\frac{N_m}{N_n}\right) \quad , \tag{51}$$

which is the gain coefficient $\kappa(\nu)$ evaluated at the center $\Delta\nu_o$ of the emission line times the ratio of bandwidth of the inverted transition to that of the probing radiation

$$\kappa = \frac{\Delta\nu o}{\Delta\nu} \kappa_o = \frac{\Delta\lambda o}{\Delta\lambda} \quad . \tag{52}$$

The gain coefficient of interest can thus be conveniently identified as

$$\kappa_o = \frac{\lambda^2}{8\pi c \Delta\nu_o} \frac{1}{\tau} N_n \left(1 - \frac{g_n}{g_m}\frac{N_m}{N_n}\right) \tag{53}$$

and the growth of intensity in transit through the medium

$$\Delta I = I_o R \kappa_o \Delta x \quad , \tag{54}$$

where

$$R = \frac{\Delta\lambda o}{\Delta\lambda} \quad \text{if} \quad \Delta\lambda \geq \Delta\lambda o$$

$$1 \quad \text{otherwise}$$

Expression (53) must be corrected to reflect the molecular structure of the transition by replacing τ with the inverse of the A-coefficient times the Franck - Condon factor, $f^+(\nu', \nu'')$. The population of the upper state N_n must be replaced with the fraction of population in the most populated rotational component

$$N_n(Jmax) = \frac{2J_m+1}{Z_r} \; N_n \quad , \tag{55}$$

where Z_r is the rotational partition function[16]

$$Z_r = \frac{\kappa T}{hcB_\nu} \quad , \tag{56}$$

where κT is the average rotational energy and B_ν is the spacing parameter for rotational levels. For the B-X band $J_m \sim 8$ and from tabulated[17,18] spectroscopic constants $(2J_{m+1})/Z_r = .134$, and $f^+ (0,0)A = 1.24 \times 10^7$, $f^+(0,1)A = 2.20 \times 10^6$, $f^+ (0,2)A = 5.01 \times 10^5$, and $f^+(0,3)A = 1.05 \times 10^5$ sec^{-1}.

To evaluate expression (53) for the various experimental conditions requires an assumption about the branching ratio for the yield of reaction (45). A lower limit can be obtained for the gain by ignoring the resonant nature of the excitation which favors the upper $B^2\Sigma_u^+$ state and assuming equal partition into the upper B and lower $X^2\Sigma_g^+$ states with the distribution among vibrational levels proportional to the Franck-Condon factors from the ground state of N_2 to the B and X states of the ion.

Collecting terms (53) becomes

$$\kappa_o \text{ max } (\nu', \nu'') = \frac{\lambda^2}{8\pi c \Delta\nu_o} \; Af^+ (\nu',\nu'') \quad (1-e^{-1}) \; X$$

$$\frac{1}{2} \; \frac{(2J_{m+1})}{Z_r} \; N_e f^B \; (\nu',0) \; \left(1 - \frac{g_n}{g_m} \; \frac{f^X(\nu'',0)}{f^B(\nu'',0)}\right) \tag{57}$$

where N_e is the initial charge density given. Values for f^B and f^X are given by Nicholls.[18]

Then, provided the lifetime for charge transfer into the states as shown in Table 4 is significantly less than the natural radiative lifetime of 66 nsec., the information from Table 3 can be used with expression (57) to give the expected small signal gain per cm. In this evaluation, the linewidth $(\Delta\lambda o)^{-1}$ has been set to 1 cm^{-1} to facilitate scaling by the unknown pressure-broadened linewidth, and resulting entries in Table 5 should be reduced by the actual linewidth in cm^{-1}. Values resulting from (57) have been halved to account for the nearly equal division of line strength between P and R branches of the spectrum.

TABLE 5

Expected gain coefficients for the $He:N_2$ plasmas parameterized in Table 3 for 20 KA excitation. Gains should be scaled by the inverse pressure--broadened linewidth $(\Delta\lambda o)^{-1}$ in cm^{-1}.

Wavelength	3914 Å	4278 Å	4709 Å	5228 Å
(ν',ν'')	(0,0)	(0,1)	(0,2)	(0,3)
Helium Pressure (Atm)				
3	-.0038	.057	.018	.0045
30	-.038	.57	.18	.045

Even in the low pressure case, the gains are high enough after the reduction in the tabulated values because of the pressure broadening to permit the extraction of stimulated emission from the plasma.

The elements of the theory just presented are sufficient to show that charge transfer reactions should provide useful laser pumping mechanisms.

The results of Table 5 indicate that, at some time after the onset of the growth of ionization in the electron beam produced plasma, the threshold for lasing can be satisfied for a cavity of practical characteristics. At that point, it can be expected the cavity will oscillate, and the resulting stimulated emission will dump as laser radiation the stored energy corresponding to the fraction of He^+ converted to N_2^+ B state molecules by that time. From Table 3 it can be seen that this output energy could be as large as 73 Joules/liter at 100 KA and 30 atm and could represent 6.8% of the energy lost by the beam in the radiating volume. However, this assumes the gas mixture can be perfectly optimized and, in practice, the filling of the lower $X^2\Sigma_g^+$ state by spontaneous emission, unfavorable branching and chemical and electrical quenching of the B state will determine a maximum effective time, τ_M, over which the charging function can be integrated to yield stored energy which can be recovered with the modelled efficiency. Because of the paucity of data describing these limiting effects, further refinement of the model to derive τ_M is unwarranted at this time. Rather, the results of parameterization of the phenomenology of test laser devices pumped by this charge transfer mechanism can serve to provide the characterizing data needed to complete the model.

However, it is important to recognize that the potentially limiting mechanisms are minimized in the charge transfer scheme described here. In this fact lies the primary advantage in this mechanism. It results primarily from the large cross sections[2], 10^{-14} cm^2, characteristic of such processes. This is to be compared with the value of 0.05×10^{-14} cm^2 characteristic of the argon-nitrogen reaction recently reported[19] to lead to laser emission in argon-nitrogen mixtures. These values are at least an order of magnitude larger than those characteristic of most excitation transfer reactions

involving neutral atomic and molecular species. This means much smaller concentrations of the gas to be excited can be used which, in turn, means that chemical quenching of the final excited state population should be virtually negligible, as seems to be the case in the nitrogen ion laser finally realized.

III. GAIN MEASUREMENTS

The entry point into the problem of evaluating the utility of charge transfer reactions as laser pumping mechanisms in plasmas excited by an e-beam discharge was felt to be in the acquisition and identification of the spontaneous emission from the proposed system. Because of its availability at the time, a Febetron 706 electron-beam device discharging single pulses of 500 KeV electrons of 3-nsec duration into a gas mixture of 3 atm of helium and a few Torr of nitrogen was used to allow spectroscopic observations of the resulting afterglows. The test gas was contained in a rectangular cell fitted with sapphire viewing windows to permit probing of a lamina of plasma transverse to and excited by primary electrons which penetrated equal distances into the cell. The optical axis was terminated on one side of the plasma by a dielectric mirror to provide in later experiments for the return of a probing laser beam.

The resulting spectrum is shown in Fig. 7 for the cases of an e-beam discharge into two samples of nitrogen, 4.9 Torr and 42.4 Torr, diluted in 3 atmospheres of helium. For the lower partial pressure of nitrogen, the spectrum shows the strong selective excitation of the $B^2\Sigma_u^+ \rightarrow X\ ^2\Sigma_g^+$ transitions of N_2^+, as expected on the basis of the discussion of Section II. Conversely, the higher partial pressure exceeds the limits set in Table 4 for a "clean" charge transfer reaction system from primary He^+ to secondary He_2^+ to $N_2^+(B^2\Sigma_u^+)$. In agreement with those expectations, intensities in the high pressure case are reduced, and there is a partition of the energy into the second Positive band system of the neutral N_2 indicating a much more complex reaction chain.

Figure 7

Survey Spectrum of the visible region made using an f/2 spectrograph. Long wavelengths are to the right. The upper spectrum for a gas mixture of 3 atmospheres of helium and 4.9 Torr N_2 shows strong selective excitation of the First Negative system of N_2^+ as expected from the discussion in Section II. The lower spectrum at the same helium pressure but a higher N_2 partial pressure (42.4 Torr) shows a considerable reduction in overall intensity and the appearance of second positive band system of the neutral N_2. As shown in Table 4, this latter case exceeds the N_2 pressure limits set for a "clean" charge transfer reaction system.

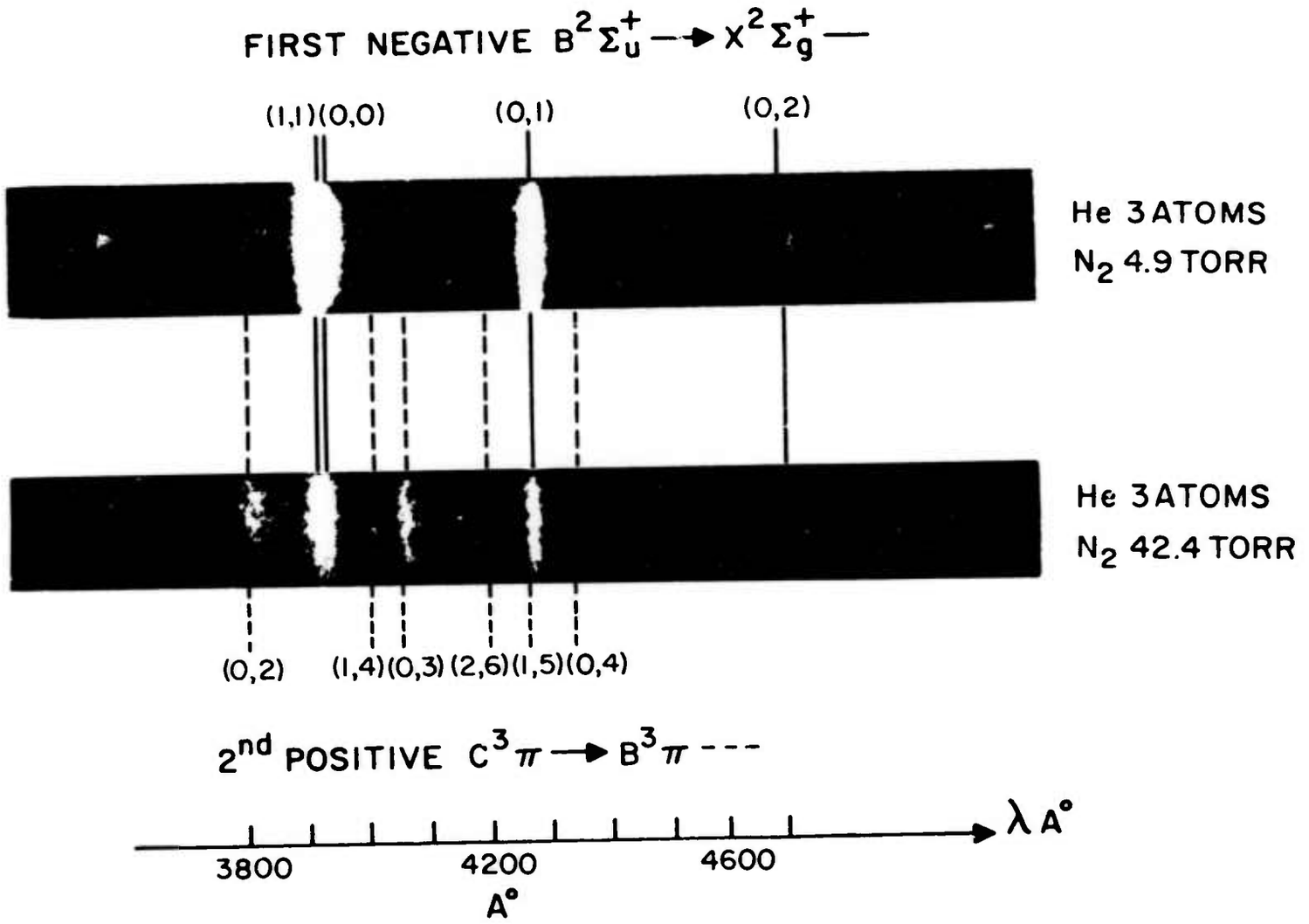
FIRST NEGATIVE $B^2\Sigma_u^+ \rightarrow X^2\Sigma_g^+$ —
(1,1)(0,0)
(0,1)
(0,2)
He 3ATOMS
N_2 4.9 TORR
He 3ATOMS
N_2 42.4 TORR
(0,2)
(1,4)(0,3)
(2,6)
(1,5)
(0,4)
2nd POSITIVE $C^3\pi \rightarrow B^3\pi$ ---
λ A°
3800
4200
4600
A°

A quantitative system for the direct measurement of gain was constructed as shown in Figure 8. Since the lifetimes for the source of molecular emissions were generally less than 100 nsec as discussed in Section II, it was necessary to use a rapidly pulsed light source for the measurement of small signal gain or absorption in a particular transition during the afterglow period. A nitrogen laser pumped, tunable dye laser with a FWHM of a few Angstroms was used in the differential path arrangement shown in Fig. 8 to measure the attenuation or amplification of the beam reflected through the plasma by the internal dielectric mirror. Use of the optical delay line in the reference path allowed for the detection of both beams with a single photomultiplier and electronics system thus minimizing the drift of the balance of sensitivity between the paths. Resulting system stability was of the order of 6% with timing jitter between the e-beam and tne dye laser small in comparison with a recombination lifetime. As accuracy of the timing measurement was around 4 nsec., adequate resolution of the particular phase of the plasma sampled by the dye laser beam could be established.

These measurements also were conducted on plasmas excited by the Febetron 706 at two current levels computed to be around 0.6 KA/cm^2 and 2.0 KA/cm^2 when the divergence of the beam and the distance to the foil window were considered. In the case of the lower current excitation, Fig. 9 shows the topology of the map of gain resulting from the measurements over the t, λ space of parameters as indicated. For each of the different vibrational transitions examined, substantial small-signal gains were recorded in both the P-branches containing the band heads and the R-branches trailing to shorter wavelengths. Units plotted are the fractional gain per

Figure 8

Experimental system for the direct measurement of gain spectra.

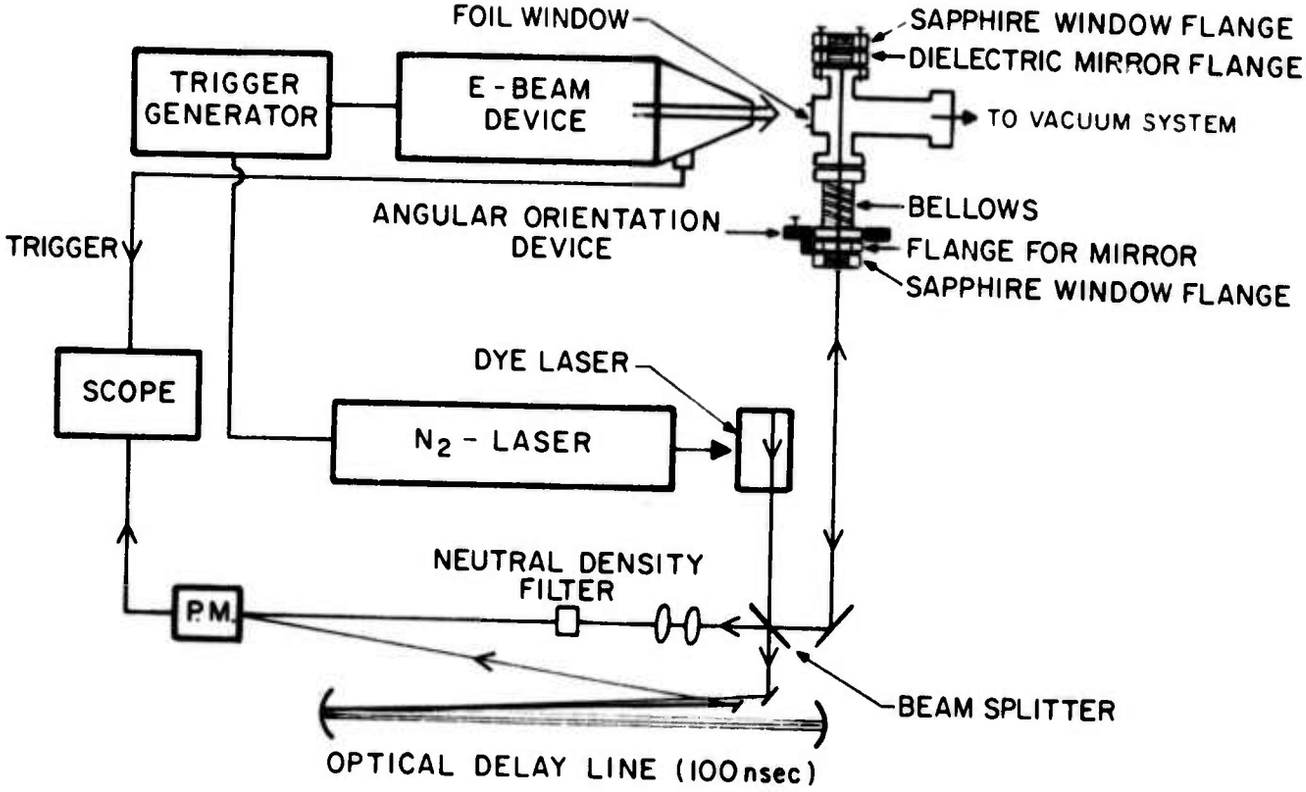
FOIL WINDOW
SAPPHIRE WINDOW FLANGE
DIELECTRIC MIRROR FLANGE
TRIGGER GENERATOR
E-BEAM DEVICE
TO VACUUM SYSTEM
BELLOWS
ANGULAR ORIENTATION DEVICE
TRIGGER
FLANGE FOR MIRROR
SAPPHIRE WINDOW FLANGE
DYE LASER
SCOPE
N_2 - LASER
NEUTRAL DENSITY FILTER
P.M.
BEAM SPLITTER
OPTICAL DELAY LINE (100nsec)

Figure 9

Fractional gain per round-trip transit of the plasma as a function of wavelength and time for the afterglow of an electron-beam discharge into 3 atm of helium containing 0.8 Torr nitrogen. Regions of stimulated emission lie above the t,λ plane; absorption below. Across the t,z plane to the rear of the data has been plotted the common time dependence of the spontaneous emission for scale. On the λ,z plane to the left edge is shown the normal spontaneous emission spectrum of the N_2^+ 1st negative bands of the $B^2\Sigma_u^+ \rightarrow X^2\Sigma_g^+$ transition, uncorrected for broadening mechanisms. The corresponding vibrational states (v',v") of the upper and lower electronic states, respectively, are shown in parentheses.

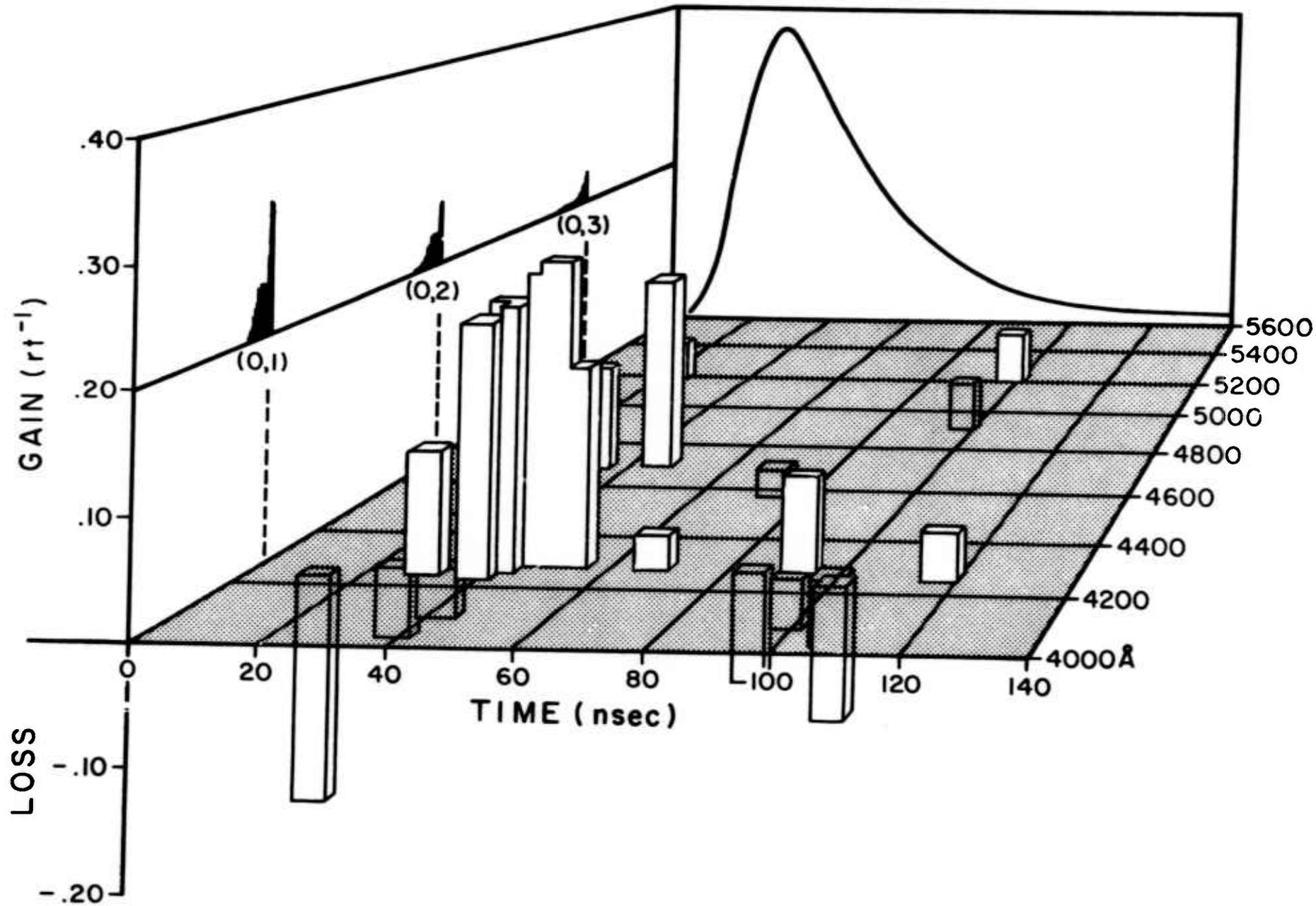
.40
.30
.20
.10
GAIN (rt⁻¹)
(0,1)
(0,2)
(0,3)
5600
5400
5200
5000
4800
4600
4400
4200
4000Å
0
20
40
60
80
100
120
140
TIME (nsec)
LOSS
-.10
-.20

round-trip transit of the afterglow. A peak gain of 0.30 at 50 nsec in the 4278 Å transition corresponds to a gain coefficient of 0.05 cm^{-1}.

As can be seen in the figure, and in greater detail in the section at 4278 Å shown in Figure 10, however, the temporal evolution of the gain coefficient was found not to be simply proportional to the upper state population as evidenced in comparison to the spontaneous emission profile shown. Later peaking of the gain suggests relaxation to the v'=0 level of some of the population of the higher vibrational states initially produced by the charge-transfer reaction (45). The same general dependence, but with decreasing amplitude was found for the (0,2) and (0,3) bands at 4709 and 5228 Å, respectively. Although data for times preceding the gain peak were quite sensitive to the precise gas composition and initial discharge current density, the occurrence and time decay of the gain were not.

Further confirmation of the magnitude of the gain was obtained from observation of the axial intensity emitted from a resonant cavity containing the plasma as a function of cavity length[20]. Cavity amplifiers were used in which the mean lifetime of a photon in the cavity considerably exceeded the lifetime of the amplifying medium. For these measurements, the dye laser was removed, and a dielectric mirror of 99% reflectance at 4278 Å was added. Optics were used having solid angles of acceptance small compared to the solid angle spanned by the forward lobe of the radiation pattern from the cavity. Under these conditions, there is no geometric effect, and the axial intensity is simply a function of the number of transits of the plasma a photon can make before the plasma decays and the

Figure 10

Time evolution of fractional gain (loss) per round trip transit of the plasma for the 4278 Å (0,1) first negative transition of N_2^+ in the afterglow of an electron beam discharge into 3 atmospheres of helium containing 0.8 Torr nitrogen.

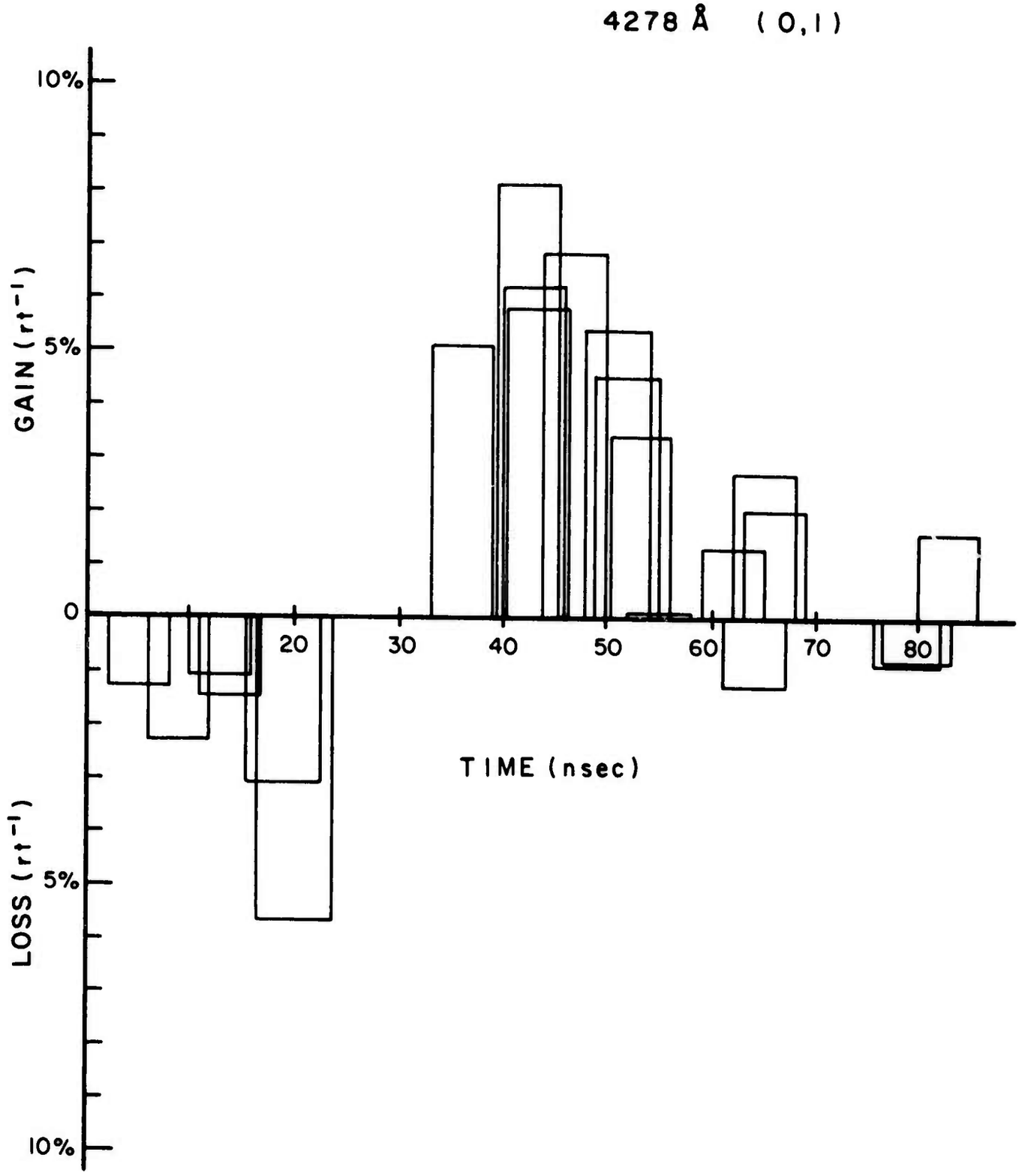
4278 Å (0,1)
10%
5%
0
5%
10%
GAIN (rt⁻¹)
LOSS (rt⁻¹)
20
30
40
50
60
70
80
TIME (nsec)

average gain or loss occurs during each transit.

Fig. 11 summarizes the resulting energy per pulse emitted axially at 4278 Å and normalized to the isotropic incoherent emission from the afterglow for cavities of four different lengths. The passive loss of the cavity was determined to be 3% per round trip from the exponential decay of the axial intensity following the termination of the afterglow. The slope of the curve of Fig. 11 is related to average net gain over the lifetime of the plasma[20], and the value of 0.02 cm^{-1} obtained is less than the peak gain seen in Fig. 9 as would be expected from the larger bandwidth of the interference filter isolating the axial emission at 4278 Å.

The measurements represented the first demonstration of the potential utility to high energy laser development of charge transfer reactions as e-beam laser pumping mechanisms and were reported in Applied Physics Letters[1]. The subsequent construction of the first nitrogen ion laser pumped by this charge transfer reaction is reported in the following section.

Figure 11

Functional dependence on the number of round-trip transits of the cavity made by a photon during the 60-nsec lifetime of the spontaneous emission of the energy emitted axially per pulse from a resonant cavity enclosing the plasma. Each measurement is normalized to the energy of the spontaneous incoherent radiation emitted at the same wavelength selected by an interference filter centered at 4264 Å with a FWHM of 57 Å

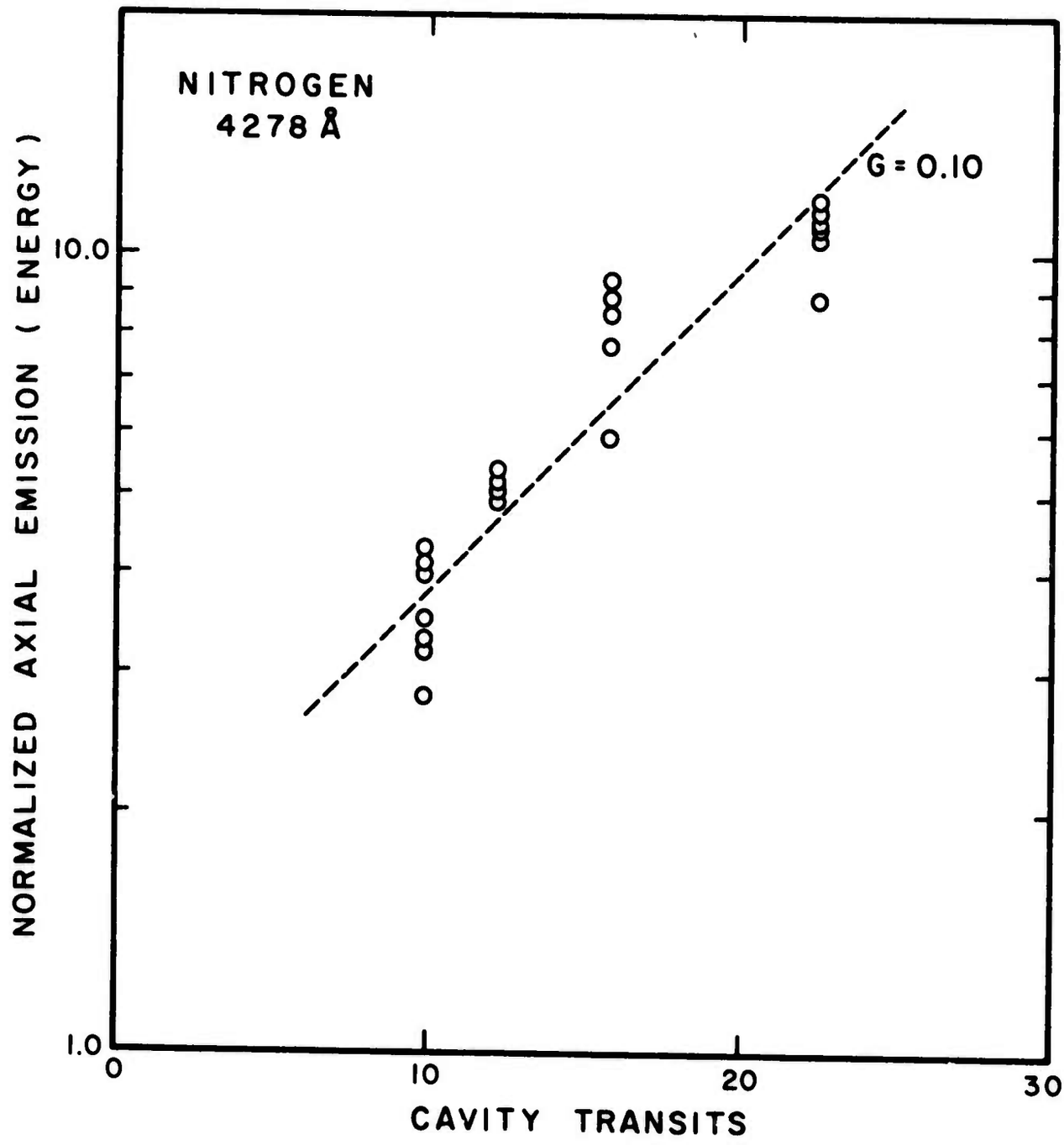
NITROGEN
4278 Å
G = 0.10
NORMALIZED AXIAL EMISSION (ENERGY)
10.0
1.0
0
10
20
30
CAVITY TRANSITS

IV. THE NITROGEN ION LASER

The series of experiments described in this section were conducted on APEX-1, the 100 KA, 1 MeV device discussed in Section II, at the manufacturer's facility prior to acceptance of the device. This experimental series was necessarily of a limited scope and designed to verify the theoretical predictions, confirmed by subsequent gain measurements, that the charge transfer reaction

$$He_2^+ + N_2 \rightarrow N_2^+(B^2\Sigma_u) + 2\,He \qquad (58)$$

held important promise as a laser pumping mechanism. In this regard, the experiments were completely successful.

The APEX-1 electron beam gun was constructed by Systems, Science and Software of Hayward, California. The device is a fast pulse, sheet beam gun emitting 100 KA pulses of 1 MeV of 1 x 10 cm transverse cross section. Pulse durations are typically 20 nanosecond FWHM with a 6.6 nanosecond rise time and a fall time controlled by a shorting electrode. By proper adjustment, the fall time can be reduced to 7 nsec. During the experimental series reported here, the anode-cathode spacing in the output diode was increased to give a larger diode impedance and consequent peak current of 13.4 KA. Larger currents were not attempted as the operation under those conditions had not been established at that time.

The afterglow chamber used in these e-beam laser experiments was necessarily different from the HPAC series[21] developed under this contract for use with the Febetron 706. The new e-beam laser afterglow chamber (ELAC-1) consisted of a laser cavity mounted to a foil support assembly and contained in a cylindrical high pressure vessel with axis of symmetry along the axis of beam propagation as shown in Figure 12. The assembly was constructed of UHV-grade stainless steel with windows and gas handling connections

Figure 12

Exploded view of the e-beam laser afterglow chamber (ELAC-1) operated as the first nitrogen ion laser.

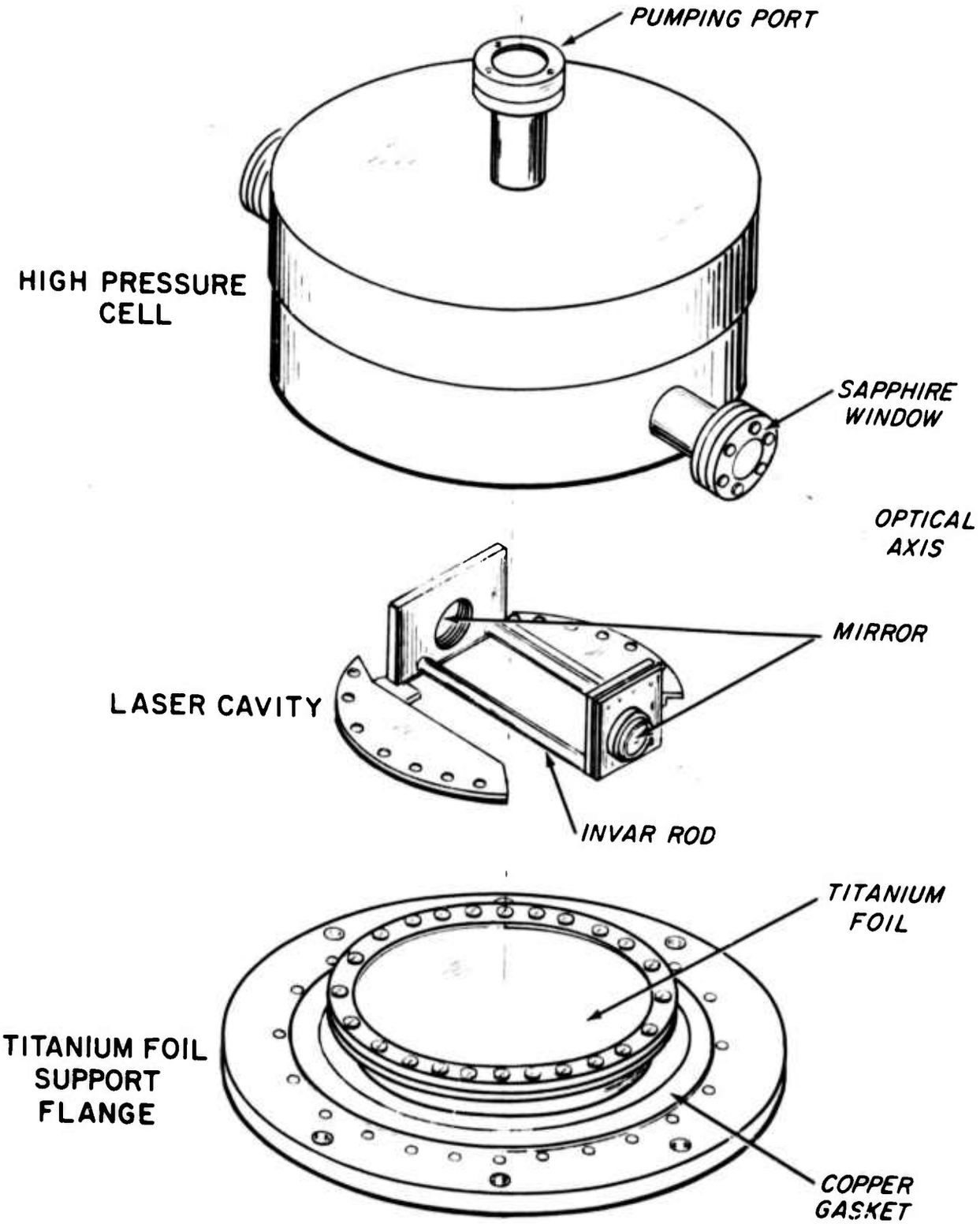
PUMPING PORT
HIGH PRESSURE CELL
SAPPHIRE WINDOW
OPTICAL AXIS
MIRROR
LASER CAVITY
INVAR ROD
TITANIUM FOIL
TITANIUM FOIL SUPPORT FLANGE
COPPER GASKET

made with Varian-type copper shear seals. The laser cavity consisted of a pair of 1 m. dielectric mirrors which were mounted to allow angular alignment, spaced with 14 cm invar rods, and contained in the pressure vessel with sapphire windows sealed across the optical axis external to the cavity as shown in Figure 12.

In operation the system was pressurized with 7 atmospheres of a mixture of helium and nitrogen. Useful partial pressures of nitrogen ranged from 2 to 20 Torr. Excitation was provided by the electron beam from APEX entering through a supported, 0.002-in. thick titanium foil window and propagating in a direction perpendicular to the optical axis.

Spectra were recorded with a scope camera focused on the image plane of a 0.25 m Jarrell Ash spectrometer with exit slit removed. Resolution was limited to 0.3 nm by the 100μ width of the entrance slit and the dispersion of the grating. The time dependence and power level of the light output was measured with a calibrated ITT F-4000, S20 vacuum photodiode connected directly to a Tektronix 519 oscilloscope. Proper attenuation of the laser output was provided by calibrated neutral density filters.

In operation, an intense violet emission from the laser could be seen on a white card placed to intersect the optical axis after it emerged from the pressure vessel. Typical operation is recorded in Fig. 13 where the white card has been replaced by a ruled translucent screen. The elliptical shape of the output spot is a result of masking of the beam by an off-axis obstruction erroneously introduced into the pressure vessel. Beam divergence was measured to be 20 milliradians from photographs of the illuminated spot on such targets successively placed at distances varying from 1 to 10 m.

Examination of the spectrum of the laser emission showed the single line

Figure 13

Emission from the first nitrogen ion laser. The output beam is seen in the photograph striking the ruled translucent target in the lower left. The emission consists of a single spectral line of less than 0.3 nm linewidth at 427 nm in the violet. The laser cavity is contained in the pressure vessel with sapphire windows sealed across the optical axis. It is the most efficient visible laser constructed to date emitting 1.8% of the electron beam energy deposited in the gas.

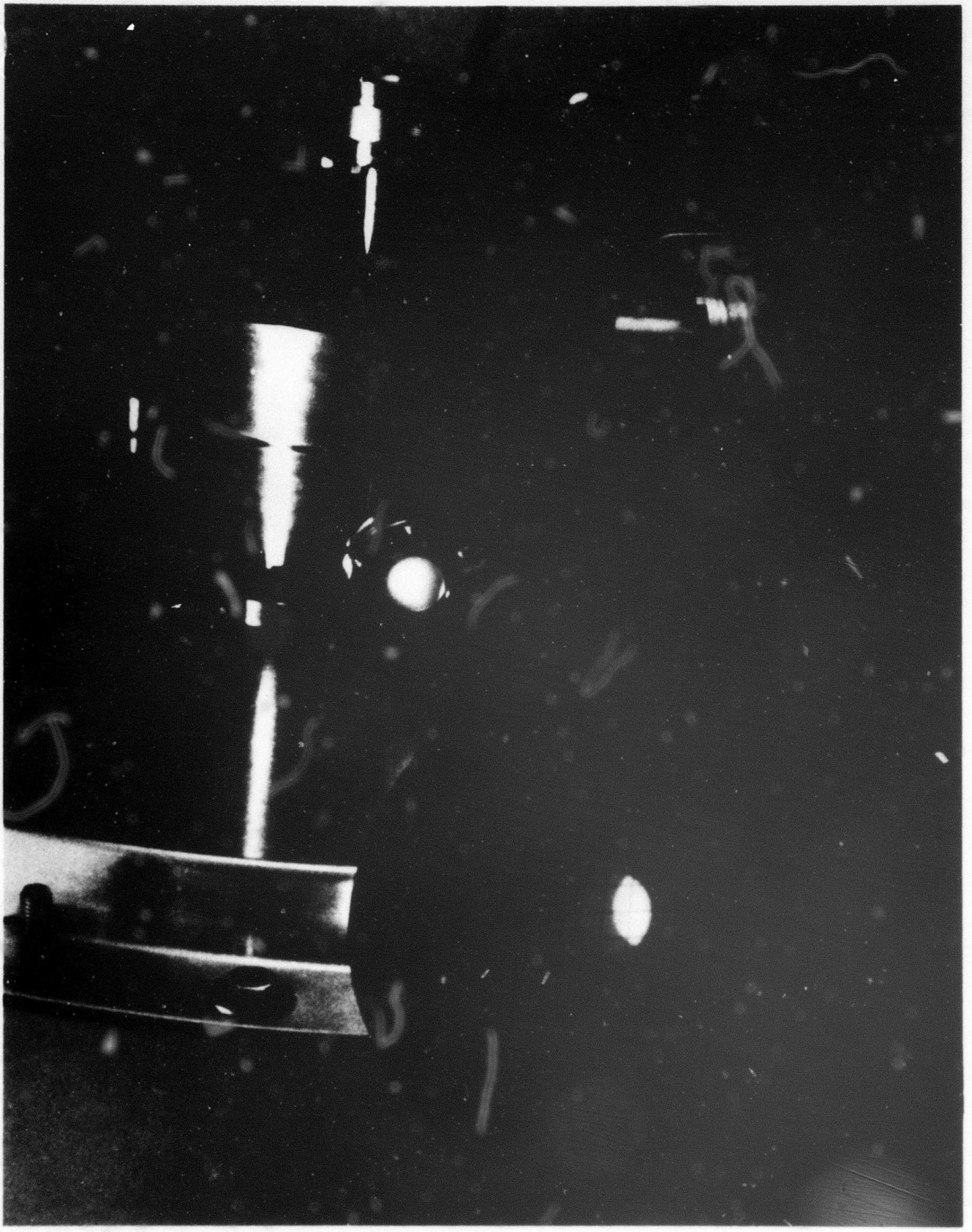

at 427 nm reproduced in Fig. 14. Reference lines at 438.8 and 447.1 nm from a separate helium discharge operated at a duty cycle 10^8 times longer were superimposed for comparison. The line at 427 nm corresponds to the band head in the P-branch of the (0,1) vibrational transition of the $B^2\Sigma_u^+ \rightarrow X^2\Sigma_g^+$ electronic transition of the nitrogen molecular ion, N_2^+. The width on the original film of the laser emission line corresponds precisely to the 0.1 mm physical width of the entrance slit and established the laser line width to be $\Delta\lambda < 0.3$ nm. Overexposure and contrast changes in reproduction have led to the slight broadening apparent in Fig. 14.

The radiating volume was estimated to be 0.625 cm^3 from application of a double cone geometry to enlarged photographs of the illuminated spot at the base of the cone on the output dielectric mirror.

A typical time-resolved power measurement is shown in Fig. 15 together with a recording of beam current plus an additive L di/dt artifact. The peak laser power shown is 9.1 KW and therefore corresponds to an emitted energy density of 0.22 J/liter. A summary of output energy as a function of nitrogen partial pressure and cavity loss per round trip transit is shown in Table 6.

Figure 14

Spectrum of the nitrogen ion laser output. The single laser line is identified at the top of the spectrum and corresponds to the 427 nm band head in the P branch of the (0,1) vibrational component of the $B^2\Sigma_u^+ \rightarrow X^2\Sigma_g^+$ electronic transition of the nitrogen molecular ion, N_2^+. Reference lines, identified below the spectrum, were superimposed from a separate helium discharge lamp of 10^8 times greater duty cycle.

LASING TRANSITION
427.8

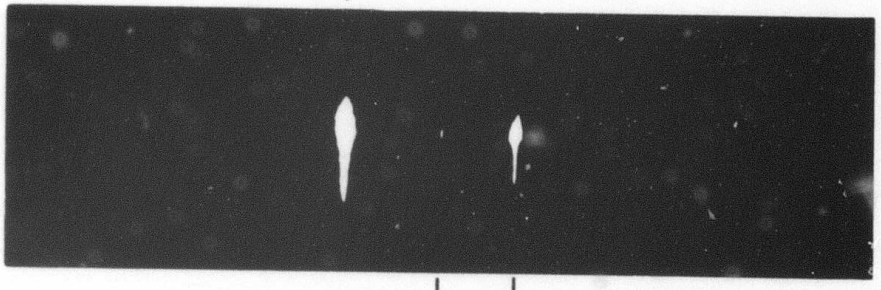

438.8 447.1
HELIUM REFERENCE SPECTRUM

Figure 15

Upper trace - Time resolved power measurement of the laser output at 10 Torr partial pressure of N_2 from a 14 cm cavity having 8.8% loss per round trip transit. Peak power corresponds to 9.1 KW. The horizontal scale is 15.8 nsec/div.

Lower trace - Time resolved record of the total electron beam current collected with a Faraday cup. Peak current density corresponds to 1.4 KA/cm^2 at 1 MV.

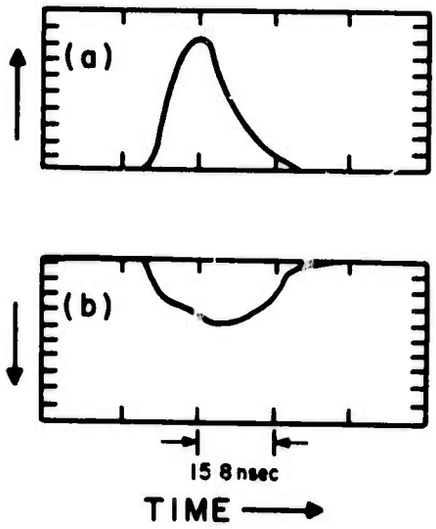

(a) Radiated Intensity
(b) Beam Current

TABLE 6

Summary of nitrogen ion laser output at 427 nm for 7 atm of helium and various partial pressures of nitrogen.

N_2 Pressure (Torr)	Mirror Losses (%/round trip)	Pulse Width (nsec)	Energy Density (Joules/liter)
2.2	19	6	.003
2.2	11.8	10	.010
2.2	8.8	14.2	.038
5.1	8.8	15.8	.208
10	8.8	15	.218
20	8.8	11	.085

In the case of the first entry in Table 6, the larger mirror losses prevented lasing until later in the afterglow period. This was seen as a pronounced displacement of the output pulse to later time. This placed a lower limit on the small signal gain of 0.01 cm^{-1} averaged over the 20 cm path length for a round trip transit.

The more nearly optimal combination of pressure and cavity losses corresponds to the trace reproduced in Fig. 15. The decay of the pulse can be seen to correspond to the ringing down time of the cavity and indicates that the total energy of the output pulse is extracted prior to the pulse maximum around 11 nsec. The energy lost by the beam during the corresponding first 11 nsec can be obtained by integrating the ionizing function F(E) shown in Fig. 5. However, since the integration limit $t \sim 11$ nsec lies in the domain $t > \tau$, eq (36) can be used.

Fig. 16 shows an enlarged representation of the timing relevant to the determination of the energy deposition from the beam. The dashed curve

Figure 16

Graphs as functions of time of the electron beam current, the corresponding calculated energy deposition and the laser output power. The dashed curve represents a linear approximation to the beam current used in the energy deposition calculations. The ordinate scale is common to all curves, and units for each are as marked.

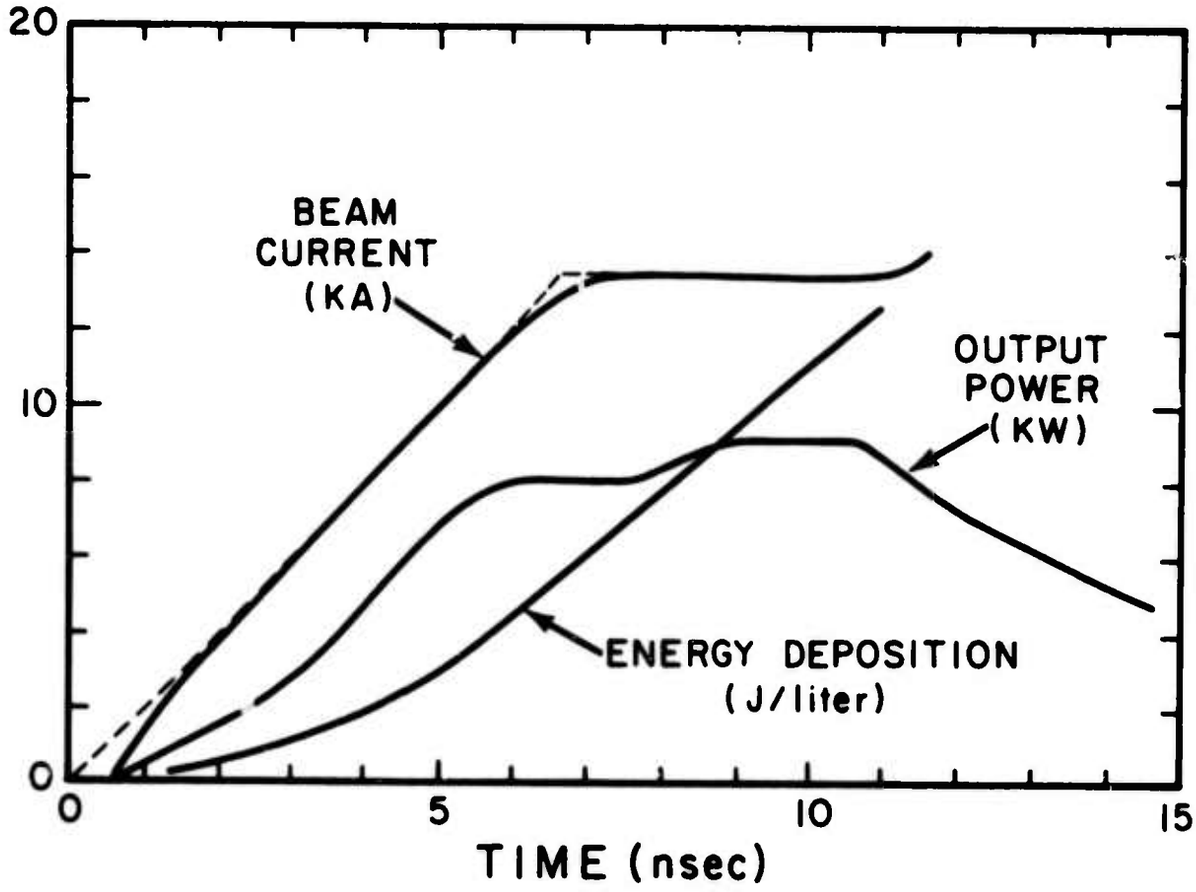
20
10
0
0
5
10
15
TIME (nsec)
BEAM
CURRENT
(KA)
OUTPUT
POWER
(KW)
ENERGY DEPOSITION
(J/liter)

represents the fit to a linear risetime used in the calculations of energy deposition. It is consistent with the sharper onset of the measured beam current seen in the figure and expected from the calculations presented in Figure 4. It appears that the "ringing down" of the output laser pulse begins about 10.8 nsec, and this time should be used in eq (36), as discussed above, to estimate the energy deposition from the beam. In this case, then,

$$\varepsilon = 12.4 \text{ Joules/liter.} \qquad (59)$$

This gives an output efficiency for 427 nm radiation of 1.8% relative to the energy lost in the radiative volume. This is to be compared with the theoretical limit of 6% for delta function, e-beam excitation at a time early enough for reaction (58) to go to completion.

As mentioned in Section II, the relevant scaling of gain for different lower state vibration components from the same v=0 upper state of the $B \rightarrow X$ transition should be roughly proportional to the product $Af^{+}(0, v'')$, where v'' is the vibrational quantum number of the lower state. From the tabulation of constants following eq (56), it can be seen that the gains for the 427, 471 and 523 nm transitions corresponding to v''=1, 2 and 3, respectively, should be in the ratio 21: 4.8: 1. Since lasing at 427 was accomplished with as much as 20% mirror loss per round trip, it should have been possible to force oscillation at 471 and 523 nm with suitable mirrors of not unrealistic characteristics.

A very brief attempt to obtain laser emission at 471 was made at the end of the experimental sequence. Using a mirror set with 36% loss per round trip at 427 nm and 1.5% at 471 nm, laser emission was observed to have a pronounced blue color. Photographs of the spot formed on a transulcent screen

made with and without interference filter peaked at 427 nm showed the laser output to be blocked by the 427 nm filter. Limitations on time and available optics prevented further experimentation along these lines, but it appears a priori that laser output at 471 has been observed. Coatings more appropriate for the purpose will be needed for future investigation and optimization of 471 nm and perhaps 523 nm emission.

V IMPLICATIONS

The high efficiency already observed for the emission of 427 nm. from the first nitrogen ion laser confirms the importance of the charge transfer pumping mechanisms proposed by the Principal Investigator and co-workers.[1] Moreover, it points toward the development, in the visible wavelength region, of new types of high energy lasers depending upon charge transfer from electron beam excitation of analogous high pressure gas mixtures. It should be emphasized that it is reasonable to expect that this will ultimately lead to the construction of lasers operating with efficiencies between 5 and 10% at a variety of wavelengths in the visible region.

More immediate implications concern the scaling of the current test laser device. If satisfactory scaling can be demonstrated in future tests of larger volumes, it is reasonable to expect that a factor of 30 can be immediately achieved in energy density output from the existing device. A factor of 7 can be expected to result from increasing the beam current from 13.4 to the maximum 100 KA and another 4.3 from increasing the pressure to 30 atm. In this case, even with no further optimization of efficiency, an output energy of 6.7 Joules/liter at 427 nm can be expected.

It is further reasonable to expect that this energy can be switched into other radiative channels from the same upper state through the use of mirror sets of appropriate reflectivity at the desired wavelength and suitably transparent at the others. Since the three potentially useful wavelengths lie at 427, 471 and 523 nm, they are sufficiently separated that fabrication of such mirror sets should present no technological problem.

Finally it appears that, if development along those lines appeared warranted, a visible laser of exceptionally high average power could be pumped by charge transfer. Assuming, again, that the test laser system proves scalable, it can be expected that some type of sustainer excitation could be arranged to pump of

the order of 30 ℓ at a repetition rate of 100 pps. Then at 6.7 J/l a laser of 20 KW average power at 427, 471, or 523 nm. could be realized. If the theoretical efficiency of 6.8% could be approached through further optimization of gas constituents, the average power output expected would increase to 75 KW.

While such projections are, of course, speculative, these are the implications of the recent successes with the first nitrogen ion laser discussed in this report.

REFERENCES

1. C. B. Collins, A. J. Cunningham, S. M. Curry, B. W. Johnson, and M. Stockton, Appl. Phys. Lett 24, 477 (1974).

2. J. B. Gerardo and A. W. Johnson, I.E.E.E., J. Quant. Elec. QE-9,748 (1973).

3. M. L. Bhaumik and E. R. Ault, U. V. Gas Laser Studies Special Technical Report (Northrop Corp. NRTC. 73-16R, (1973)).

4. R. W. Dreyfus and R. T. Hodgson, Appl. Phys. Lett. 20, 195 (1972).

5. R. T. Hodgson and R. W. Dreyfus, Phys. Rev. Lett. 28, 536 (1973).

6. D. A. Hammer and N. Rostoker, Phys. Fluids 13, 1831 (1970).

7. R. V. Lovelace and R. M. Sudan, Phys. Rev. Lett. 27, 1256 (1971).

8. G. Knop and W. Paul, in: Alpha, Beta and Gamma-Ray Spectroscopy (ed. Kai Siegbahn, North-Holland Co., Amsterdam, 1965), p 1-25.

9. W. P. Jesse and J. Sadauskis, Phys. Rev. 97, 1668 (1955).

10. C. B. Collins and W. W. Robertson, J. Chem. Phys. 40, 701 (1964).

11. R. A. Gerber, G. F. Sauter and H. J. Oskam, Phys. Lett., 19, 656 (1966).

12. D. K. Bohme, N. G. Adams, M. Mosesman, D. B. Dunkin, and E. E. Ferguson, J. Chem. Phys. 52, 5094 (1970).

13. F. C. Fehsenfeld, P. D. Goldan, A. L. Schmettekoph, H. I. Schiff, and E. E. Ferguson, J. Chem. Phys. 44 4087 (1966).

14. G. Herzberg, Molecular Spectra and Molecular Structure: I. Spectra of Diatomic Molecules (Van Nostrand, Princeton, N. J., 1950), p. 21.

15. D. C. Tyte and R. W. Nicholls, Identification Atlas of Molecular Spectra, University of W. Ontario, Dept. of Physics, Molecular Excitation Group, London, Ont. 1965 p. 14.

16. G. Herzberg, op. cit., p. 125.

17. G. Herzberg, op. cit., p. 554

18. R. W. Nicholls, J. Res. NBS, 65A, 451, (1961).

19. M.L. Bhaumik, E.R. Ault, and N.T. Olson, U.V. Gas Laser Investigations Semi-annual Technical Report (Northrop Corp, NRTC. 74-26R, (May 1974)).

20. C. B. Collins, A. J. Cunningham, S. M. Curry, B. W. Johnson, and M. Stockton, Appl. Phys. Lett. 24, 245 (1974).

21. C. B. Collins and A. J. Cunningham, Recombination Laser, Report No. UTDP A002-4, ONR Contract No. N00014-67-A-0310-0007, 1974.

ACKNOWLEDGEMENT

The authors gratefully acknowledge the assistance of System Science and Software personnel throughout the experiments reported in Section IV which were performed at System Science and Software facility in Hayward, California.

The assistance of Dr. M. Stockton and members of The University of Texas at Dallas high energy laser group in performing these experiments is further acknowledged.

APPENDIX I

Manuscript copy of, "A Nitrogen Ion Laser Pumped by Charge Transfer," by C. B. Collins, A. J. Cunningham, and M. Stockton, Appl. Phys. Lett. (pend.)

A nitrogen ion laser pumped by charge transfer*

C. B. Collins, A. J. Cunningham, and M. Stockton

The University of Texas at Dallas, Richardson, Texas 75080

The first nitrogen ion laser pumped by charge transfer from He_2^+ is reported in this work. Intense laser emission in the violet at 427 nm has been observed and found to have a linewidth less than 0.3 nm. The pumping ion, He_2^+, was produced by discharge of a fast-pulsed electron beam gun, APEX-1, into 7 atm of a mixture of helium and nitrogen. Excitation current densities were 1.4 kA/cm^2 at 1 MV over a 1×10 cm transverse geometry. Under these conditions, the efficiency of the emission of 427-nm laser radiation was found to be 1.9% relative to the energy lost by the electron beam in the radiating volume.

It was recently suggested by Collins *et al.*[1] that resonant charge transfer reactions might provide nearly ideal pumping mechanisms for recovering one photon for each ion produced by the discharge of an intense electron beam into high pressure gas. Since the energy from an electron-beam discharge can be stored at densities of the order of kilojoules per liter with efficiencies over 50%, such a pumping mechanism would clearly point toward the development of electron-beam lasers operating at visible wavelengths with system efficiencies between 5 and 10%. The potential of the pumping reaction

$$He_2^+ + N_2 \rightarrow N_2^+(B^2\Sigma_u^+) + 2He, \qquad (1)$$

was reported in the same letter, together with construction of a two-pass amplifier excited by a Febetron 706 and operating at 427.8, 470.9, and 522.8 nm.[1] This letter reports construction and operation of the first nitrogen ion laser pumped by reaction (1). Intense laser emission at 427 nm was produced with an efficiency of 1.9% relative to the energy lost by the electron beam in the radiating volume.

The laser device used in these experiments consisted of a pair of 1-m dielectric mirrors which were mounted to allow angular alignment, spaced with 14-cm Invar rods, and contained in a stainless steel pressure vessel with sapphire windows sealed across the optical axis external to the cavity. In operation the system was pressurized with 7 atm of a mixture of helium and nitrogen. Useful partial pressures of nitrogen ranged from 2 to 20 Torr. Excitation was provided by an electron beam entering through a supported, 0.002-in.-thick titanium foil window and propagating in a direction perpendicular to the optical axis. The cross section of the beam was 1×10 cm with the longer transverse axis coincident with the optical axis of the cavity. The electron beam was emitted by APEX-1 and pulsed at 14 kA and 950 kV for a duration of 20 nsec with rise and fall times of 7 nsec.

Spectra were recorded with a scope camera focused on the image plane of a 0.25-m Jarrell Ash spectrometer with exit slits removed. Resolution was limited to 0.3 nm by the width of the entrance slit and the dispersion of the grating. The time dependence and power level of the light output was measured with a calibrated ITT F-4000, S20 vacuum photodiode connected directly to a Tektronix 519 oscilloscope. Proper attenuation of the laser output was provided by calibrated neutral density filters.

In operation an intense violet emission from the laser could be seen on a white card placed to intersect the optical axis after it emerged from the pressure vessel. Beam divergence was measured to be 20 mrad from photographs of the illuminated spot on targets successively placed at distances varying from 1 to 10 m.

Examination of the spectrum of the laser emission showed the single line at 427 nm reproduced in Fig. 1. Reference lines at 438.8 and 447.1 nm from a separate helium discharge operated at a duty cycle 10^3 times longer were superimposed for comparison. The line at 427 nm corresponds to the band head in the P branch of the (0, 1) vibrational transition of the $B^2\Sigma_u^+ - X^2\Sigma_g^+$ electronic transition of the nitrogen molecular ion N_2^+. The width on the original film of the laser emission line corresponds precisely to the 0.1 mm physical width of the entrance slit and established the laser linewidth to be $\Delta\lambda < 0.3$ nm. Overexposure and contrast changes in reproduction have led to the slight broadening apparent in Fig. 1.

The radiating volume was estimated to be 0.5 cm^3 from application of a double cone geometry to enlarged photographs of the illuminated spot at the base of the cone on the output dielectric mirror.

A typical time-resolved power measurement is shown in Fig. 2 together with a recording of beam current plus an additive $L(di/dt)$ artifact. The peak laser power

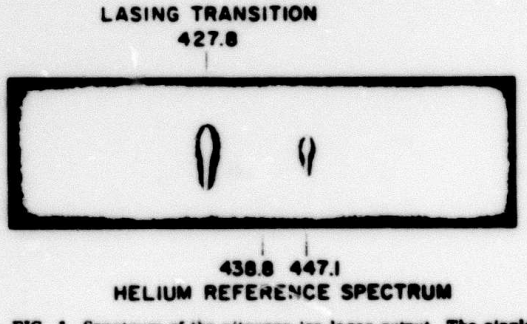

FIG. 1. Spectrum of the nitrogen ion laser output. The single laser line is identified at the top of the spectrum and corresponds to the 427-nm band head in the P branch of the (0,1) vibrational component of the $B^2\Sigma_u^+ - X^2\Sigma_g^+$ electronic transition of the nitrogen molecular ion N_2^+. Reference lines, identified below the spectrum, were superimposed from a separate helium discharge lamp of 10^3 times greater duty cycle.

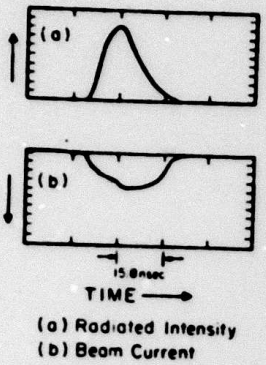

FIG. 2. Upper trace: Time-resolved power measurement of the laser output at 10 Torr partial pressure of N_2 from a 14-cm cavity having 8.8% loss per round-trip transit. Peak power corresponds to 9.1 kW. The horizontal scale is 15.8 nsec/div. Lower trace: Time-resolved record of the total electron-beam current collected with a Faraday cup. Peak current density corresponds to 1.4 kA/cm^2 at 1 MV. The first maximum is an $L(di/dt)$ artifact.

shown is 9.1 kW and therefore corresponds to an emitted energy density of 0.27 J/liter. A summary of output energy as a function of nitrogen partial pressure and cavity loss per round-trip transit is shown in Table I.

In the case of the first entry in Table I, the larger mirror losses prevented lasing until later in the afterglow period. This was seen as a pronounced displacement of the output pulse to later time. This placed a lower limit on the small signal gain of 0.01 cm^{-1} averaged over the 20 cm path length for a round-trip transit.

The more nearly optimal combination of pressure cavity losses corresponds to the trace reproduced in Fig. 2. The decay of the pulse can be seen to correspond to the ringing down time of the cavity and indicates that the total energy of the output pulse is extracted prior to the pulse maximum at 7 nsec. The energy lost by the beam during the corresponding first 7 nsec

TABLE I. Summary of nitrogen ion laser output at 427 nm for 7 atm of helium and various partial pressures of nitrogen.

N_2 pressure (Torr)	Mirror losses (ℓ m^{-1})	Pulse width (nsec)	Energy density (J/liter)
2.2	19	6	0.004
2.2	11.8	10	0.012
2.2	8.8	14.2	0.048
5.1	8.8	15.8	0.260
10	8.8	15	0.272
20	8.8	11	0.106

can be calculated from range-energy consideration to be 14.4 J/liter. This gives an output efficiency for 427-nm radiation of 1.9% relative to beam energy lost in the radiating volume. This is to be compared with the theoretical limit of 6.5% for delta function, electron-beam excitation at a time early enough for reaction (1) to go to completion.

In conclusion, it appears the work reported here confirms the importance of charge transfer reactions as laser pumping mechanisms. In particular, the high efficiency for the emission of 427-nm laser radiation from the system discussed above evidently points to the importance of the nitrogen ion laser as a device of considerable significance.

*Research supported by the U.S. Advanced Research Projects Agency of the Department of Defense and monitored by ONR under contract No. N00014-67-A-0310-0007.

[1]C.B. Collins, A.J. Cunningham, S.M. Curry, B.W. Johnson, and M. Stockton, Appl. Phys. Lett. 24, 477 (1974).